



Sediment geochemistry of the section Tagay-1 at Olkhon Island (Lake Baikal, Eastern Siberia): a contribution to palaeoenvironmental interpretations

Varvara V. Ivanova^{1,3} · Alexander A. Shchetnikov^{2,3,4,5} · Steffen Kiel⁶

Received: 25 August 2022 / Revised: 25 October 2022 / Accepted: 14 November 2022 / Published online: 14 December 2022
© The Author(s) 2022

Abstract

The Miocene Tagay section in the north-western part of Olkhon Island, Lake Baikal, provides a unique window into past life in northern Asia. To aid palaeoenvironmental reconstructions, we carried out whole-rock geochemical analyses of 17 sedimentary layers of this section. The aim of this geochemical approach is to examine the element variations as a response to climate change during formation of the Tagay section deposits with a focus on the hydrological regime of the catchment and in-lake processes. Our results establish that temperature and climate conditions during the formation of sediments of section Tagay-1 were fairly stable, no abrupt climatic changes occurred. The palaeoclimate was temperate, however, it had a cyclic nature: wet and semiarid epochs of different intensity and duration alternated. The basal part of the sediment sequence is dominated by terrigenous material, mainly by surface runoff, so the sedimentation was fed by erosion products of the weathering crust. During sedimentation of this lower part (layers 17–9), the palaeo-lake level and salinity stayed practically unchanged. The drawdown of the palaeo-lake and increasing salinity started in the higher middle part (layer 8), and reached the minimum water level and maximum salinity in layers 7–6. Sediments of the layers 8–6 accumulated in an arid climate. After deposition of layer 5, the water level began to rise, and during formation of layer 3 it fell again. The highest sedimentation rate was in layers 12–5, these are also the layers with the highest enrichment of biogenic elements (layers 12, 7–5) and where carbonate deposition took place. The observed changes in element behaviour are related to hydrological changes in the catchment (precipitation), lake level status, and evaporation, and are ultimately driven by climate.

This article is a contribution to the special issue “The Miocene Tagay locality of Olkhon Island (Lake Baikal, Eastern Siberia) – a multidisciplinary approach”

Keywords Baikal · Sediment geochemistry · Authigenic minerals · Rare elements · Diagenesis · Palaeoclimate

✉ Varvara V. Ivanova
vargeo66@gmail.com

✉ Steffen Kiel
steffen.kiel@nrm.se

- ¹ Federal State Budgetary Institution “Academician I.S. Gramberg All-Russian Scientific Research Institute for Geology and Mineral Resources of the Ocean” (FSBI “VNIIOkeangeologia”), 1, Angliysky Av., St. Petersburg 190121, Russia
- ² Institute of the Earth’s Crust, Siberian Branch, Russian Academy of Sciences, Lermontova str. 128, Irkutsk 664033, Russia
- ³ Geological Institute, Russian Academy of Sciences, Pyzhevsky lane 7, Moscow 119017, Russia
- ⁴ A.P. Vinogradov Institute of Geochemistry, Siberian Branch, Russian Academy of Sciences, Favorskogo str. 1a, Irkutsk 664033, Russia
- ⁵ Laboratory of Geoarchaeology of Baikal Siberia, Irkutsk State University, 5 Armii str. 52, Irkutsk 664025, Russia
- ⁶ Department of Palaeobiology, Swedish Museum of Natural History, Box 50007, 104 05 Stockholm, Sweden

Introduction

The Miocene Tagay section located in the northwestern part of the Olkhon Island (Fig. 1) in Lake Baikal, Siberia, is a unique window into the terrestrial fossil record of northern Asia. It represents the northernmost locality for Miocene terrestrial fossils on the entire Eurasian continent and the most important of such sites in Siberia (Daxner-Höck et al. 2013). Palaeontological research indicates that the Tagay section provides evidence for the exchange between European and Asian floral and faunal elements adapted to humid climate, at a time when central Asia was already as arid as it is today (Erbajeva and Alexeeva 2013).

The geologic and palaeontological importance of the Tagay locality has been known since the mid 50’s of the last century (Kitaynik 1958). The first detailed geologic description of the Tagay section and its fauna and flora was presented

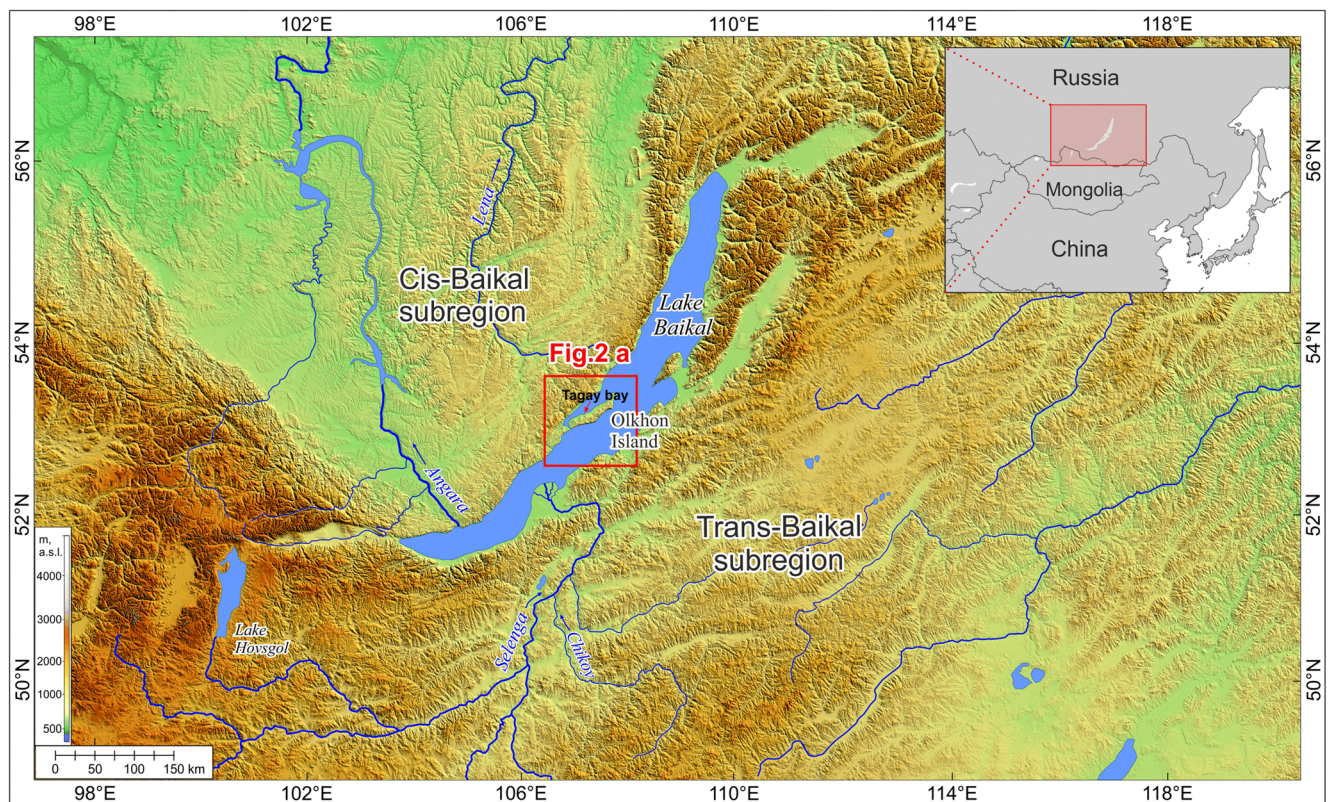


Fig. 1 Digital relief map of the Baikal region and position of Tagay Bay on Olkhon Island (see also Fig. 2 a in Daxner-Höck et al. (2022), this issue). Data from SRTM v.4 was used in the design of the diagram with a resolution of 90 m

by Logachev et al. (1964). Geological, geomorphologic and palaeontological investigations followed (Logachev 1974; Mats et al. 1982; Mats et al. 2001; Vislobokova 1990, 1994, 2004; Kossler 2003; Pokatilov 2004; Daxner-Höck et al. 2013). The palaeontological record culminated in a rich collection of fossil fishes, amphibians, lizards, snakes, turtles, birds and mammals, that were excavated in the course of field campaigns of the Russian Academy of Sciences between 2012 and 2016 (Filippov et al. 2000; Danilov et al. 2012; Zelenkov and Martynovich 2013; Syromyatnikova 2014, 2015, 2016; Klementiev and Sizov 2015; Sizov and Klementiev 2015; Tesakov and Lopatin 2015; Zelenkov 2015, 2016a,b; Zelenkov et al. 2018; Sotnikova et al. 2019; Čerňanský et al. 2020; Volkova 2020). The recent palaeontological findings show no visible evolution of the mammalian species occurring within the Tagay-1 section, indicating that the sediments were deposited within a short time of ~200 Kyr (Daxner-Höck et al. 2022, this issue).

In this paper we aim at a multidisciplinary approach to the Tagay locality, specifically to the Neogene sediment sequence of the Tagay Formation (Mats et al. 2011), that is exposed along section Tagay-1 at Tagay Bay (coordinates 53° 9'34.74"N, 107° 12'43.12"E). The relevant fieldwork was carried out in summer 2014 by a team of international specialists from Siberia, Austria and Mongolia. We decided to locate our new cross-section close to the Tagay section published by Logachev et al.

(1964), which allows reliable correlation of the stratigraphic sequence, comparison of lithologies of sediment layers and the fossil content of both the published and the new Tagay-1 section. Among other topics, the new multidisciplinary investigations focus on the palaeomagnetic pattern along the section, secondly, on the biostratigraphically relevant small mammal-record of the fossil-bearing sediment layers, and finally, on age dating of the mammal fauna by correlation of biostratigraphic and magnetostratigraphic data and the Geologic Time Scale.

The reconstruction of palaeoenvironments and palaeoclimate will be based on the palaeontological record and on sedimentary and geochemical data. The aim of our geochemical approach is to examine the element variations as a response to climate change during formation of the Tagay section deposits with focus on the hydrological regime of the catchment and in-lake processes. Special attention is given to the investigation of element distributions and their change over time and to reconstruction of trends in sediment input, lake level, carbonate precipitation, redox and acid-alkaline conditions, bioproductivity, and palaeoclimate based on geochemical proxies

Lithostratigraphy

The Tagay section is composed of variegated (green, black, brown) clays that are strongly lithified at the base of the

section, with horizons of calcareous nodules, interlayers of sands and silts with inclusions of gruss and rubbles¹. Sediment sorting is poor, the ratio of fine to coarse fractions in the sediments varies widely, and the clays contain various inclusions. Even the most homogeneous clays contain 2–8% silt-sand admixture. These clays are, according to Logachev et al. (1964), polymineralic mixtures of kaolinite-hydromicaceous-montmorillonite with a predominance of iron-magnesium montmorillonite over other clay minerals. The mineral composition of the heavy fraction of sediments is dominated by garnet, ilmenite, rutile, manganese hydroxides, apatite, zircon, and epidote. The light fraction is dominated by quartz and feldspars. An important feature of the deposits is their high carbonate content. Carbonates are presented as individual horizons of limestone and marls, as well as impurities and nodules in clays (Kitaynik 1958; Logachev et al. 1964; Mats et al. 2010).

The package of Cenozoic sediments has a slight inclination of 5–7° in a southwestern direction. In general, the bedding of sediments is parallel, gently undulating, and lenticular. The apparent thickness of the sediments of section is 12 m. The bedrocks, which are submerged under the water level of Lake Baikal, are represented by Palaeozoic metamorphic complexes, mainly biotite gneisses and migmatites with deep pockets of the weathering crust (Mats et al. 2001). We identified 17 separate layers in the Tagay section. Layers 3–10 contain a large variety of animal remains, including fishes, reptiles, birds, mammals and snails. Below is a layer-by-layer description of the Tagay section (from top to bottom) (Table 1, Fig. 2):

Materials and Methods

To identify the geochemical composition of the Tagay sediments, whole rock geochemical analyses were performed on 59 samples collected at a spacing of 0.2 m through the entire profile. The quantifications and major element weathering and pedogenic indices described below were used to perform palaeoclimatic reconstructions through the Tagay section.

Determination of the rock-forming elements, oxides, and trace elements (Sc, V, Cr, Co, Ni, Cu, Zn, Ga, Rb, Sr, Y, Zr, Nb, Mo, Ba, Pb, Th, U) was made using X-ray fluorescence (XRF) at the Institute of Earth's Crust, Irkutsk, with the methods described by Pashkova et al. (2018). Loss on ignition (LOI) measurements were done at 1000°C. Oxide content analysis results were recalculated as a percentage of dry weight after the samples were ignited, and then to the molar mass for primary whole rock geochemistry parameter

evaluation (Nesbitt and Young 1982). Analysis of rare earth elements (REE) and trace elements, including the ones from the REE group in a subset of 18 samples, corresponding to the main lithological units of the section (Fig. 2), was made using the ICP-MS method (IGC SB RAS, Irkutsk) with relative error of 5–10% as described in Panteeva et al. (2003). Analytical results were statistically treated with the Statistica 10.0 software. Analysis of the range of major element weathering and pedogenic indices through the section (Table 2) was made for a general description of the deposits.

In order to determine the degree of weathering, we used the Chemical Index of Alteration: $CIA = (Al_2O_3 / (Al_2O_3 + CaO^* + Na_2O + K_2O)) * 100$ (Nesbitt and Young 1982), where CaO^* represents CaO in silicate-bearing minerals only; and the index of compositional variability: $ICV = (Fe_2O_3 + K_2O + Na_2O + CaO + MgO + TiO_2) / Al_2O_3$ (Cox et al. 1995). The Tagay sediments contain variable amounts of carbonate minerals and this is reflected by variable LOI results. The Chemical Index of Alteration (CIA) (Nesbitt and Young 1982) basically measures the amount of feldspar relative to clay minerals, and requires calculation of non-carbonate Ca, which is almost impossible in carbonate-rich sediments. CaO from non-silicate minerals (carbonate and phosphate) is excluded using the methodology proposed by McLennan (1994). The content of corrected CaO is calculated as $CaO_{rest} = CaO - (10/3) * P_2O_5$; if $CaO_{rest} < Na_2O$, then the content of $CaO^* = CaO_{rest}$, otherwise, $CaO^* = Na_2O$.

Nesbitt and Young (1982) indicated that the influence of weathering processes at the source on the composition of clastic sediments can also be detected using the A–CN–K diagram [= molar $(Al_2O_3 - (CaO^* + Na_2O) - K_2O)$], where CaO^* represents the amount of CaO entering into the structure of silicate minerals. We use this diagram for the Tagay sediments. The ICV includes Fe, Mg, and Mn, and does not require calculation of non-carbonate Ca (Cox et al. 1995).

The degree of element accumulation in the sediments was estimated as an Enrichment Factor (EF). EF values were calculated according to Turgeon and Brumsack (2006), by normalizing all elements contents in the sediments by the content of the reference element Al. Concentrations are compared to the average shale values (Wedepohl 1991) and expressed as enrichment factors ($EF_{element}$) relative to average shale. Enrichment factors were calculated using:

$$EF_{element} = (element/Al)_{sample} \div (element/Al)_{shale} \quad (1)$$

SiO_2 and CaO excess values (Si_{ex} and Ca_{ex} , respectively), i.e. Si and Ca levels above “normal” detrital background, were determined using the general formula:

$$Element_{ex} = Element_{sample} - [(Element/Al)_{background} \times Al_{sample}], \quad (2)$$

¹ Gruss is a sediment of mixed grain size resulting from the chemical and mechanical weathering of crystalline rocks. Rubble is a broken stone, of irregular size, shape and texture.

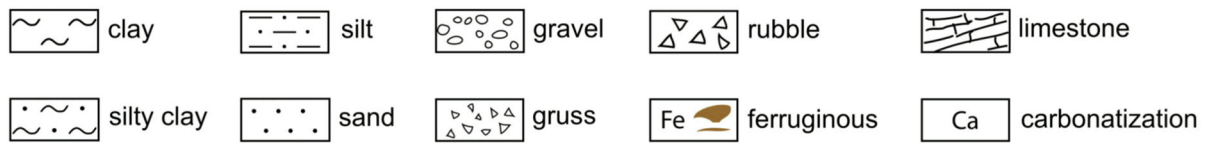
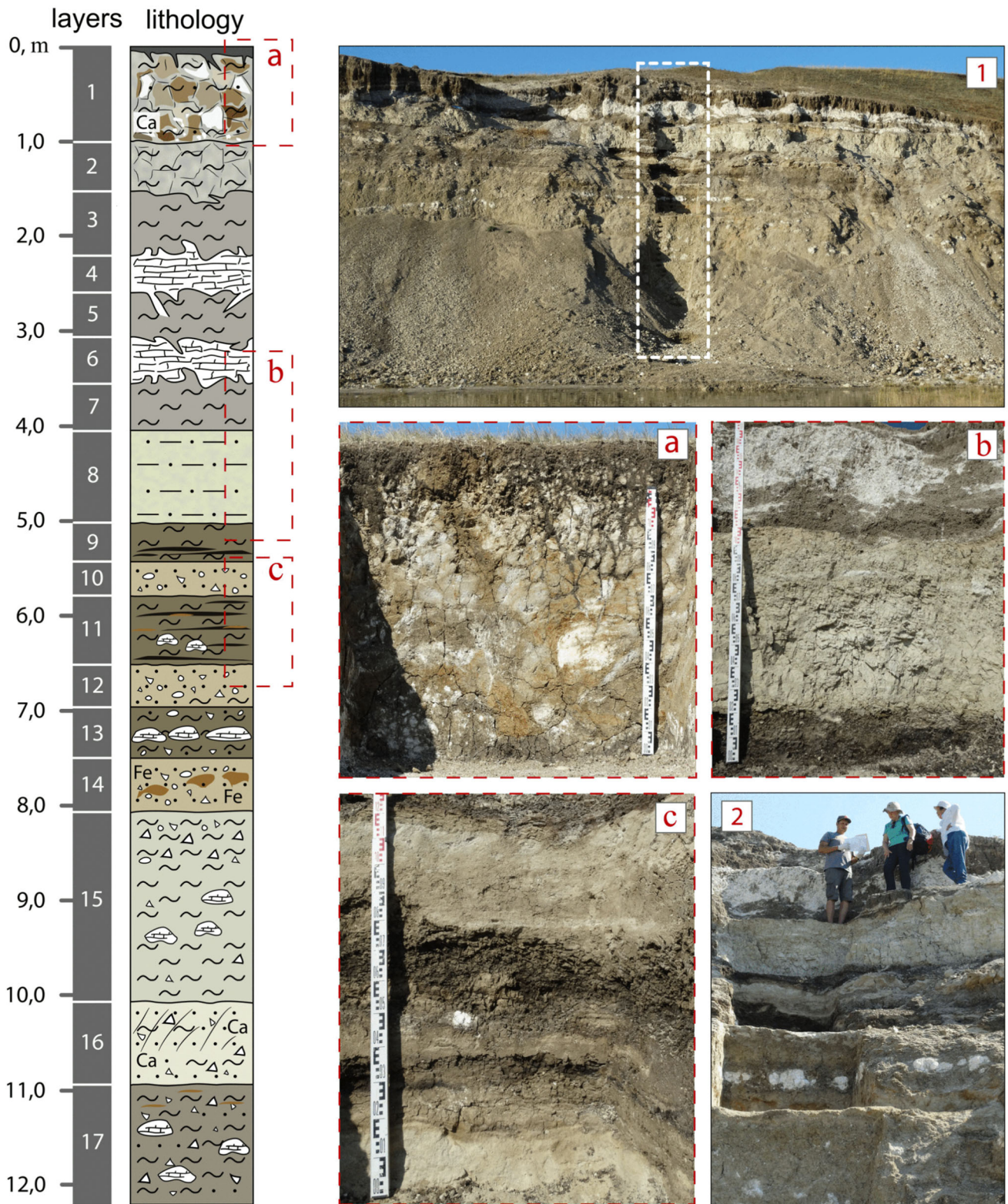
Table 1 Description of the lithological column of the Tagay-1 section (from top to bottom)

Layer, №	Description	Thickness, m
1	Variegated (red, white, gray, brown) sandy clays with chaotically scattered spots and lenses of silt (leopard texture), non-layered, sometimes ferruginous, covered with a dense network of cracks filled with modern soils. The sediments of the layer are residual deposits over Tertiary clays, which had been formed since the end of Tertiary sedimentogenesis to the present. The boundary with the underlying layer is very uneven and indistinct.	0.7-1.0
2	Light brown due to ferruginization and dark gray clays and silt with spots of white soft limestone, admixture of gruss and sand; at the base of the layer, a poorly expressed hollow wavy bedding appears. The border with the underlying layer is jagged tom, pocket-like.	0.4-0.6
3	Dark green clays, dense, massive, plastic, with numerous inclusions of randomly distributed white carbonate concretions. The contact is clear, very uneven, with lace penetrations into the underlying sediments. <i>Fossil remains (Pisces, Reptilia)</i> .	0.5-0.7
4	White lumpy limestone of pelitic composition, in places with a strong degree of lithification in the form of carbonate nodules, with spots and lacy-shaped lenses of dark gray, almost black clays, lenticular-bedded. The layer has a variable thickness, wedges out on the flanks of the section. The basal contact is uneven, with intrusions into the underlying sediments.	0.2-0.8
5	Yellowish-green, slightly sandy clays, strongly fractured. The base is irregular with deep uneven penetrations into the underlying layer. The deposits contain numerous inclusions of bone remains. <i>Many fossil remains (Pisces, Reptilia, Gastropoda, Aves, Mammalia)</i>	0.5
6	White soft limestone of pelitic composition, sandy, in places with a strong degree of lithification in the form of carbonate nodules. The layer has a variable thickness, wedges out. The base of the layer has a jagged, uneven contact; the deposits of the overlying and underlying layers penetrate deeply into it. <i>Fossil remains (Pisces, Amphibia, Reptilia)</i> .	0.3-0.5
7	Dark green sandy clays, lacy texture, with numerous inclusions of randomly distributed white carbonate aggregates. The layer has variable thickness. The base is clear, gently undulating. <i>Fossil remains (Pisces, Reptilia, Gastropoda, Aves, Mammalia)</i> .	0.2-0.5
8	Light green homogeneous silt in the upper part with a brownish tint and weakly expressed parallel bedding, fine-platy structure, which becomes coarsely lumpy towards the base of the layer, here in some places elements of vertical columnar jointing are observed. The lower boundary is clear, gently undulating, occasionally with small lenticular and in the form of spots injections into the underlying layer.	1.0 m
9	Brown and dark brown clays, layered owing to colour change. The upper and lower parts of the layer are lighter. The base of the layer is clear, gently wavy. <i>Fossil remains (Pisces, Reptilia, Gastropoda, Aves, Mammalia)</i> .	0.4
10	Yellowish-green mixed-grained sand, unstratified and unsorted, with inclusions of gravel and gruss. The base of the layer has a straight, sharp contact. <i>Fossil remains (Gastropoda, Pisces, Amphibia)</i> .	0.4
11	Brown clays, layered due to changes in colour and lithological composition, sandy layers are replaced by clay in the total mass, and there are horizons of white carbonate nodules and lenses of orange-ocher loam. The base is clear, gently wavy.	0.8
12	Yellow-gray mixed-grained sands with gravel, gruss, fine gravel. Lenses of dark green clays are present. Poorly sorted clayey sands at the bottom. The base is clear, gently wavy.	0.4
13	Dark green clay with a horizon of white limestone nodules. At the top and bottom of the layer, an admixture of mixed-grained sand, gravel, and gruss is added to the clays. The base is clear, gently wavy.	0.6
14	Yellowish-gray sands of various grains with gravel, grit, fine gravel, unsorted, non-layered. Due to iron hydroxides, rusty streaks and spots are observed. The base is gently wavy.	0.5
15	Light green clays, very dense due to lithification, with rubble and gravel. In the upper part of the layer, the highest concentration of admixtures of gravel, gruss, and sand. In the middle part of the layer, there are spots of white soft limestone. The base of the layer is poorly expressed, uneven.	2.1
16	Light green sands, clayey, with spots of soft limestone, slightly ochreous due to impregnation with iron hydroxides, with the inclusion of gruss, rubble, weathered quartz, granite. The contact with the underlying layer is uneven, gradational.	0.8
17	Dark green, very dense clay due to significant lithification, sandy with a large number of rubble inclusions, gruss, with numerous nodules (concretions) of white limestone.	1.3

where (element/Al) background is the ratio between the element and Al in detrital material. For Si and Ca, a first order approximation is provided using the background Si/Al value of 3.08 and the Ca/Al value of 0.56 (Mats et al. 2010). The non-detrital Si and Ca concentrations, calculated according to (1) have negative values for five samples (carbonate levels: layers 4 and 6), indicating that the Element/Al ratio in detrital material in this area is somewhat lower than in general in the region. To avoid negative values when calculating the average Si and Ca content per sample, the non-detrital concentration

was corrected to the lowest ratio in the sediment sequence (Peinerud et al. 2001).

Fig. 2 Lithological column of the Tagay section (left) and photos of the spotty texture of weathering crust formed on Miocene clays in the top of the section (**a**), as well as characteristic structural elements of the middle part of the section (**b** and **c**). The position of the excavation against the general background of the section (1, dashed rectangle) and its upper part, where the main bone-bearing horizons are concentrated (2). For a detailed description of units 1 to 17, please refer to Table 1. Photos by the authors



The Sr/Ba ratio was calculated to estimate the salinity of the water body, with increasing values suggesting an increase in salinity (Zhao et al. 2019). The Sr/Ca-ratio might reflect evaporational environmental stress resulting in periodic draw-down of the lake (Heymann et al. 2013). The Sr/Ca-ratios for shallow-water sediments will be lower than for deep-water sediments.

The FM ($\text{Fe}_2\text{O}_3 + \text{MnO} + \text{MgO}/\text{SiO}_2$) - NAM ($\text{Na}_2\text{O} + \text{K}_2\text{O}/\text{Al}_2\text{O}_3$) module diagram (Yudovich and Ketris 2000) and the K/Al-Mg/Al diagram (Turgeon and Brumsack 2006) were used to characterise the mineral composition of the sediments. Inferences about the original clay mineralogy can be made using the methodology of Kackstaetter (2014). Oxide content analysis results were recalculated to normative minerals using SEDMIN, a Microsoft Excel spreadsheet for calculating fine-grained sedimentary rock mineralogy from bulk geochemical analysis (Kackstaetter 2014).

The ternary diagram proposed by Erofeev and Tsekhovskii (1983) was used to distinguish arid and subarid depositional environments. We have further used a binary elemental ratio–ratio proxy model ($\text{K}_2\text{O}/\text{Al}_2\text{O}_3$ vs. Ga/Rb) (cf., Roy and Roser 2013) to reconstruct the palaeoclimatic history of the sediments. Ratios of the redox-sensitive elements V/(V+Ni), Ni/Co, V/Cr; Fe/Mn and binary diagram of V/Cr–Ni/Co were applied for detailed investigations of the past lake water column properties (Maslov 2005; Bulkan et al. 2019).

To unravel REE behaviour during the formation of the Tagay sedimentary sequence, we applied the REE signature diagrams - patterns of chondrite-normalized REE concentrations, which allow comparison of the concentration, distribution, and the degree of REE fractionation in each sample (Anders and Grevesse 1989). Then, the geochemical differences between the sediments were investigated using the following criteria:

- Ce^* , Eu^* , Pr^* - value of cerium, europium and praseodymium anomaly, expressed as $\text{Ce}^* = 3\text{Ce}_N/(2\text{La}_N + \text{Nd}_N)$ (Taylor and McLennan 1985); $\text{Eu}^* = 2\text{Eu}_N/(\text{Sm}_N + \text{Gd}_N)$ (Balashov 1976); $\text{Pr}^* = 2\text{Pr}_N/(\text{Ce}_N + \text{Nd}_N)$ (Patrick et al., 2004); (subscript N = NASC-normalized values, Gromet et al. 1984);
- $\Sigma\text{REE} + \text{Y}$ – the total content of REEs and yttrium (Balashov 1976); ΣLREE , ΣMREE and ΣHREE -content of the light (La-Nd), middle (Sm-Dy) and heavy (Er-Lu) REEs, respectively.
- $\Sigma\text{Ce}/\Sigma\text{Y}$, where ΣCe (La - Gd), ΣY (Tb - Lu, Y) the index marking the intensity of weathering on land, where feldspars and accessory Ce-minerals disintegrate more intensely under humid lithogenesis, which results in a $\Sigma\text{Ce}/\Sigma\text{Y}$ increase. (Balashov 1976);
- ratio of LREE/HREE, expressed as $((\text{La} + \text{Pr} + \text{Nd})/(\text{Er} + \text{Tm} + \text{Yb} + \text{Lu}))_{\text{sample}} / ((\text{La} + \text{Pr} + \text{Nd})/(\text{Er} + \text{Tm} + \text{Yb} + \text{Lu}))_N$ (Maslov et al. 2007) (subscript N = NASC-

Table 2 Major element weathering and pedogenic indices

Index	Calculation	Proxy information	Pedogenic process	Reference
HM	$\frac{\text{Al}_2\text{O}_3 + \text{TiO}_2 + \text{Fe}_2\text{O}_3 + \text{FeO} + \text{MnO}}{\text{SiO}_2}$	Hydrolizate index. Intensity of chemical weathering	Hydrolysis	Yudovich and Ketris, 2000; Maslov, 2005;
TM	$\frac{\text{TiO}_2}{\text{Al}_2\text{O}_3}$	Titanium index. Ti is most readily removed by physical weathering, Al by chemical weathering. Acidification (provenance)	Acidification	Yudovich and Ketris, 2000; Maslov, 2005; Sheldon, 2006
SM	$\frac{\text{Na}_2\text{O}}{\text{Al}_2\text{O}_3}$	Sodium index. Intensity of chemical weathering: degradation of plagioclases.	Alkali elements accumulate as soluble salts not removed: salinization	Yudovich and Ketris, 2000; Maslov, 2005; Retallack, 2007
AM	$\frac{\text{Na}_2\text{O}}{\text{K}_2\text{O}}$	Alkaline index. The ratio is a signal of the K-feldspar and mica content versus plagioclase content in the sediments.	Salinization	Yudovich and Ketris, 2000; Maslov, 2005; Retallack, 2007
NAM	$\frac{(\text{Na}_2\text{O} + \text{K}_2\text{O})}{\text{Al}_2\text{O}_3}$	Normalized alkalinity index. Prevalence of feldspars. Provenance (presence of basic volcanic rocks)-high values.	Salinization	Yudovich and Ketris, 2000; Maslov, 2005; Retallack, 2001; Sheldon and Tabor, 2009
ASM	$\frac{\text{Al}_2\text{O}_3}{\text{SiO}_2}$	Alumosilicic index. Degree of weathering. Clayeyness. Al accumulated as clay minerals form	Hydrolysis	Yudovich and Ketris, 2000; Maslov, 2005; Sheldon and Tabor, 2009
FM	$\frac{(\text{Fe}_2\text{O}_3 + \text{MnO} + \text{MgO})}{\text{SiO}_2}$	Femic index. Diagnosis of polymineral clays, in which four common clay minerals (hydromica, chlorite, montmorillonite, and kaolinite) form mixtures of two to three, and often all four minerals.	Salinization	Yudovich and Ketris, 2000; Maslov, 2005

normalized values) – characterises the degree of carbonation. Light lanthanides isomorphically substitute Ca in the lattice of carbonate minerals (Kučera et al. 2009);

- $(La/Yb)_N$, $(La/Sm)_N$, - indicators of the facies sediment accumulation conditions (Trueman et al. 2006) (subscript N = NASC-normalized values).

As an additional criterion of changes in the LREE/HREE abundances, the magnitude of the tetrad effect of lanthanide fractionation was used for the 3rd and 4th tetrads. The tetrad effect is the spectrum infraction of REE concentrations normalized to chondrite, expressed in splitting the entire spectrum into groups (tetrads) with formation of a zigzag-shaped line: La–Ce–Pr–Nd, Pm–Sm–Eu–Gd, Gd–Tb–Dy–Ho, and Er–Tm–Yb–Lu. For each tetrad in the REE spectrum, curves are formed with the boundaries between Nd and Sm, on Gd and between Ho and Er (McLennan 1994). The tetrad effect can be treated similarly to the quantification of Ce or Eu anomalies in logarithmic representations (Irber 1999) as equation 3:

$$ti = \sqrt{\frac{v1 \times v4}{v2 \times v3}} \quad (3)$$

in which v_1 , v_2 , v_3 and v_4 are the normalized concentrations of 1st, 2nd, 3rd and 4th lanthanide in each individual tetrad. The concave segments of the tetrad are called W-type effect, whereas convex segments are called M-type effect (McLennan 1994). In a solution, the W-type effect results from the complex REE compound foundation, equilibrium with the colloidal hydroxyl compounds Fe and Mn, and the presence of slightly reduced conditions (Dia et al. 2000). Values of tetrad effect significantly larger than 1 indicate that the M-type pattern occurs, while values significantly lower than 1 indicate the W-type effect.

The samples are housed in the Geological Institute of Ulan-Ude and Irkutsk Institute of the Earth's Crust.

Results

Statistical features of the distribution of major oxides, loss on ignition (LOI) (%) and trace elements in the Miocene sediments of the Tagay section are shown in Table 3. This table also provides information about statistical features of the distribution of major element weathering and pedogenic indices.

Fluctuating values of the main rock-forming oxides and trace elements are observed in the samples retrieved from the Tagay section. The sediments reveal relatively low to moderate variations in composition. They are characterised by a relatively low SiO₂ content (median 60.4%), ranging from 23.3% to 84% with low (21%) variation. Al₂O₃ concentrations show only

minor variations, with a median of 17.6%. The concentrations of TiO₂ are relatively high, with a median of 0.6%. The CaO, MnO, and MgO contents vary rather widely, with median concentrations of 1.6%, 0.1%, and 1.6%, respectively. The studied deposits are characterised by relatively low contents of Na₂O, K₂O, and P₂O₅. The LOI varies from 0.9% to 19%. The major element weathering and pedogenic indices demonstrate low and moderate variations. The distribution of trace elements also shows moderate variations with the exceptions of Rb and Sr. Extreme contents of some elements (such as Al, Mn, Mg, Ca, P, Ba, and K) are observed in the samples retrieved from layers 4, 5, 6, 8, 9, 10, 15 and 17 (numbered according to the lithostratigraphic section in Fig. 2 (left)).

A summary of the Enrichment Factors (EF) calculated using Equation 1 is provided in Table 4.

The calculated EF values show that the sediments are on average depleted in all components except for Ca, Ba, and Zr. The high “carbonate” layers 4, 5, 6 are anomalously enriched in Mn, Mg, Ca, P, and Ba.

The trend of silicate weathering is displayed graphically on the Al₂O₃–(CaO*+Na₂O)–K₂O diagram (Nesbitt 2003) (Fig. 3).

Figure 4(a, b) illustrates the mineral composition of the clayey sediments of the Tagay section. These plots allow us to distinguish six main lithochemical types of clay rocks, differing in the mineral composition of the clay fraction.

The location of the composition points of the section deposits in the Erofeev–Tsekhovskii diagram (Erofeev and Tsekhovskii 1983) and in the binary diagram Ga/Rb–K₂O/Al₂O₃ (Roy and Roser 2013) are shown on the Figs. 5 and 6.

Normative mineralogical calculations from bulk geochemistry of the Tagay sediments suggest that quartz, gypsum, apatite, albite, rutile, hematite, calcite, montmorillonite (smectite), sericite, chlorite and kaolinite are present. Only five samples contain too much carbonate for the calculations to be meaningful. The quartz content in the suitable samples ranges from 26% to 68%, calcite ranges from 4% to 75%, with clays dominated by sericite, illite, montmorillonite (smectite) and chlorite. Figure 7 shows the distribution of normative quartz, calcite, gypsum, smectite, chlorite, and kaolinite through the Tagay profile.

Figure 8(a, b) shows the variations of the EF and major element weathering indices with depth. All distribution curves were smoothed by the moving average method with a window of 4. Analysis of distribution patterns allows for the section's geochemical stratification.

In addition to investigations of the element concentrations, distribution of V/Cr, U/Th, Ni/Co, V/(V+Ni), Mn/Fe (smoothed with moving average), and cross-correlation of V/Cr–Ni/Co were applied for the assessment of the past lake water column redox properties (Bulkan et al. 2019) (Figs. 9, and 10).

Table 3 Statistical features of the distribution of major oxides, LOI (%), trace elements (ppm) and petrochemical indices in the Miocene sediments of the Tagay-1 section

Oxide (element, index)	Valid N*	Mean	Median	Minimum	Maximum	Std.Dev.	Coef.Var.
SiO ₂	56	60.4	60.4	23.3	84.0	12.5	21
TiO ₂	59	0.6	0.6	0.1	1.0	0.3	45
Al ₂ O ₃	54	17.1	17.6	8.9	24.4	3.5	20
Fe ₂ O ₃ tot.	59	5.9	5.7	1.0	11.7	3.0	51
MnO	55	0.1	0.1	0.0	0.2	0.1	84
MgO	58	1.8	1.6	0.3	4.3	1.0	57
CaO	51	2.2	1.6	0.8	6.2	1.3	58
Na ₂ O	55	0.8	0.8	0.3	1.6	0.4	44
K ₂ O	50	1.2	1.2	0.6	1.8	0.2	19
P ₂ O ₅	55	0.1	0.1	0.0	0.5	0.1	81
LOI	55	8.0	7.8	0.9	19.0	4.2	52
HM	59	0.45	0.42	0.14	0.74	0.17	37
TM	55	0.04	0.04	0.02	0.05	0.01	24
ASM	55	0.29	0.27	0.11	0.48	0.10	33
SM	58	0.04	0.04	0.00	0.10	0.03	61
NAM	59	0.12	0.11	0.05	0.21	0.04	31
AM	55	0.59	0.52	0.00	1.41	0.32	55
CIA	55	71	74	44	86	9	13
PIA	58	74	77	44	90	10	14
ICV	54	0.57	0.49	0.30	1.74	0.24	43
Si _{ex}	54	7.07	5.20	0.14	24.78	5.9	72
Ca _{ex}	45	1.07	0.70	0.11	3.79	0.89	83
S	54	0.022	0.017	0.006	0.068	0.016	74
Ni	54	23	20	9	65	11	48
Cu	56	28	25	10	70	13	47
Zn	59	76	60	10	210	43	56
Pb	58	18	18	5	27	4	24
V	59	107	110	10	200	45	42
Cr	59	48	48	9	77	12	26
Co	58	15	13	5	38	7	49
Sc	59	15	16	2	25	5	32
Ba	48	669	550	96	1700	326	49
Sr	52	225	210	140	400	66	29
Y	57	17	15	7	40	8	46
Zr	59	195	190	10	410	95	49
Rb	59	44	36	3	160	33	76
Th	59	9	9	4	21	3	36
U	58	4	4	3	10	2	43

*Extremes and outliers were removed from dataset.

Table 5 provides REE composition of the Tagay section sediments.

The data in Table 5 show that the contents of REE are characterised by moderate variations, and the contents of elements of the light (La-Nd) group are less variable in relation to the medium (Sm-Ho) and heavy (Er-Lu) elements. Chondrite-normalized REE patterns in the Tagay section sediments

compared to the REE patterns of various bedrocks of Olkhon Island are shown in Fig. 11.

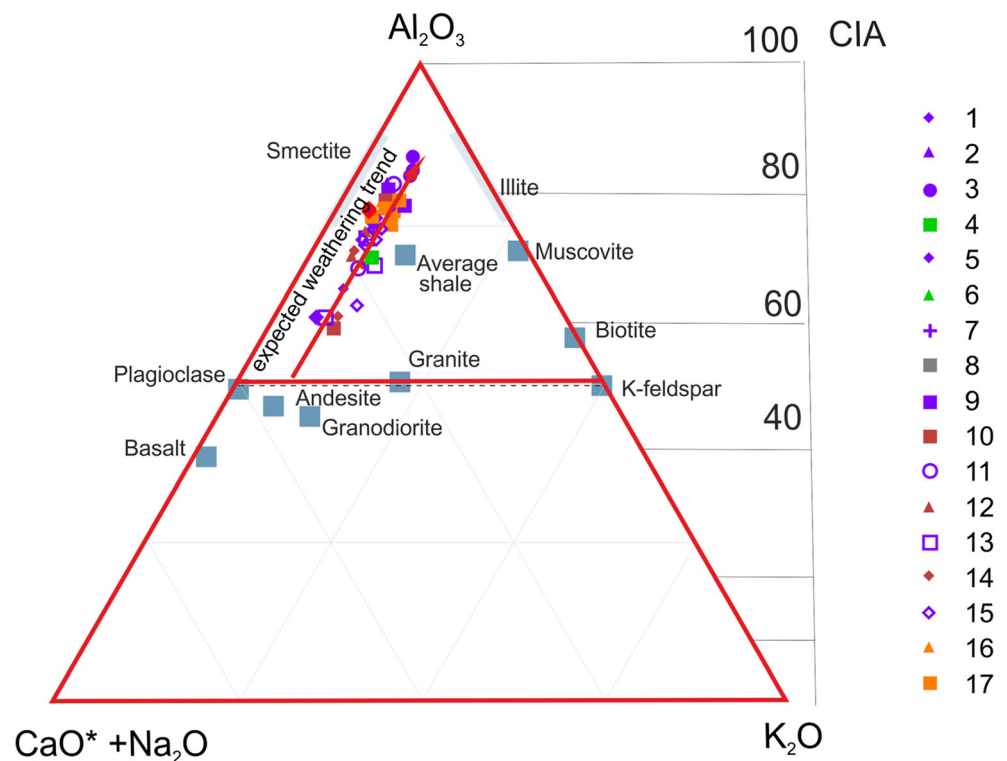
The true positive and negative cerium anomalies were used to clarify the depositional conditions. (Fig. 12). True cerium anomalies are those that are not affected by lanthanum concentrations; negative anomalies will plot above approximately 1.05 on the x-axis (praseodymium

Table 4 Statistical features of the distribution of the Enrichment Factors (EF) in the Miocene sediments of the Tagay-1 section

EF	Valid N*	Mean	Median	Minimum	Maximum	Std.Dev.	Coef.Var.
Si	59	1.01	0.92	0.53	2.39	0.44	44
Ti	59	0.69	0.71	0.06	1.04	0.19	27
Fe	59	0.82	0.80	0.25	1.51	0.33	40
Mn	53	0.56	0.47	0.10	1.91	0.42	76
Mg	54	0.64	0.59	0.18	1.79	0.38	59
Ca	54	1.04	0.73	0.28	4.49	0.90	86
Na	55	0.63	0.50	0.20	2.07	0.44	70
K	59	0.38	0.36	0.18	0.68	0.10	26
P	51	0.69	0.58	0.16	2.29	0.53	77
Ni	59	0.37	0.27	0.15	1.36	0.26	70
Cu	59	0.66	0.51	0.29	2.77	0.39	59
Zn	59	0.82	0.65	0.17	2.23	0.50	61
Pb	59	0.92	0.85	0.61	1.73	0.25	28
V	59	0.78	0.74	0.38	1.74	0.24	31
Cr	59	0.54	0.51	0.31	1.18	0.19	35
Co	48	0.68	0.60	0.26	1.67	0.32	48
Sc	52	1.00	1.01	0.24	1.68	0.27	27
Ba	56	1.09	1.00	0.16	2.21	0.48	44
Sr	59	0.89	0.70	0.35	4.77	0.76	86
Y	59	0.68	0.59	0.26	2.04	0.35	52
Zr	59	1.20	1.23	0.07	2.65	0.56	47
Th	59	0.80	0.71	0.45	1.92	0.30	37
U	17	0.96	0.74	0.60	2.67	0.53	56
Rb	58	0.27	0.23	0.07	0.73	0.15	54

*Extremes and outliers were removed from dataset.

Fig. 3 Ternary plot of the chemical index of alteration (CIA) and A-CN-K ($Al_2O_3 - CaO^* + Na_2O - K_2O$) diagram (Nesbitt 2003), for the sedimentary rocks of the Tagay section. Average rock and mineral values are from McLennan et al. (1993) and Pettijohn (1975). Layers are numbered according to the lithostratigraphic section in Fig. 2 (left). Similar types of rocks are highlighted in violet (clays); green (limestones); grey (silts); brown (sands); orange (silty clays)



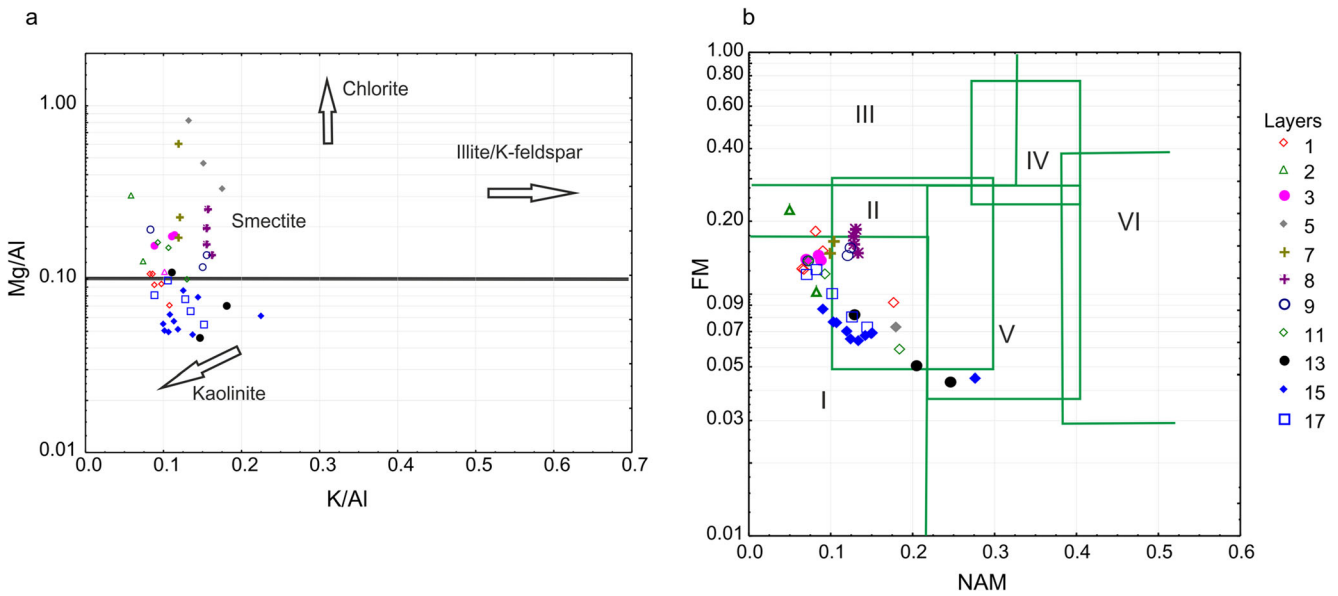


Fig. 4 a Plot of Mg/Al vs. K/Al (A). b FM ((Fe₂O₃+MnO+MgO)/SiO₂)—NAM ((Na₂O+K₂O)/Al₂O₃) module diagram (Yudovich and Ketris 2000). I–VI, clay minerals in the fields are: I, kaolinite, II, montmorillonite with minor abundance of kaolinite and hydromica, III, chlorite with minor abundance of Fe-hydromica, IV, chlorite and hydromica;

V, chlorite, montmorillonite, and hydromica (with abundant mixed-layer minerals); VI, hydromica with appreciable amount of potassium feldspar. Layers are numbered according to the lithostratigraphic section in Fig. 2 (left)

anomaly) and below approximately 0.95 on the y-axis (cerium anomaly) (Patrick et al. 2004). True positive cerium anomalies will plot below approximately 0.95 on the x-axis and above approximately 1.05 on the y-axis (Patrick et al. 2004).

The La_N/Yb_N – La_N/Sm_N cross-correlation obtained for the Tagay section sediments is shown in Fig. 13 and was used to aid in environmental reconstructions (Trueman et al. 2006).

Figure 14 shows variations of the REE geochemical coefficients along the Tagay profile.

Fig. 5 Erofeev–Tsekhovskii diagram for the Tagay sediments. Layers are numbered according to the lithostratigraphic section in Fig. 2 (left). Similar types of rocks are highlighted in violet (clays); green (limestones); grey (silts); brown (sands); orange (silty clays)

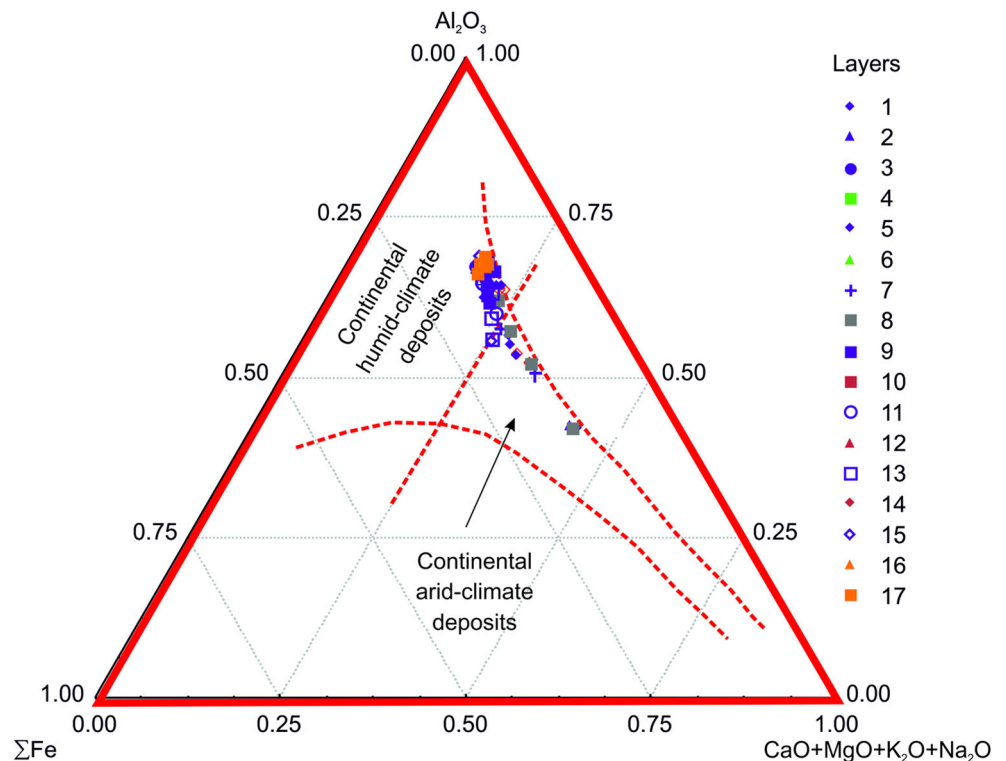
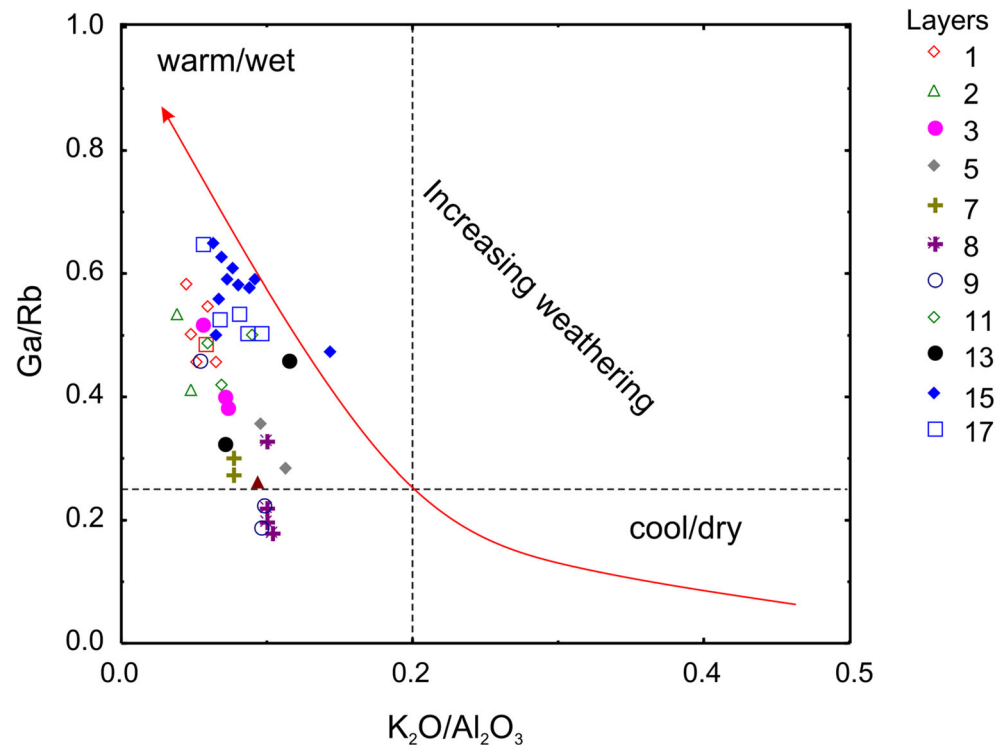


Fig. 6 Ga/Rb-K₂O/Al₂O₃ plot for the clayey sediments (Tagay section). Layers are numbered according to the lithostratigraphic section in Fig. 2 (left)



Discussion

Whole rock geochemistry and assessment of the palaeoenvironment

Given the autochthonous sedimentation in the Olkhon area (Logachev et al. 1964; Mats et al. 2010), the removal of terrigenous material was mainly the result of surface runoff, so that the sedimentary basin was mainly fed by erosion products of the weathering crust of the kaolinite and montmorillonite type. This factor determines the composition of the deposits. The concentrations of the main rock-forming oxides and major element weathering and pedogenic index values in most samples correspond to the values of these parameters in the source area rocks (Mats et al. 2010). This observation and the relatively low to moderate variations in the sediment composition reflect a low degree of the chemical alteration. It can be assumed that a) the sediment sequence formed in a geologically short time; and b) no abrupt climatic changes occurred during deposition.

LOI is affected by sediment composition. One of the most influential factor is the lattice water in clays that can account for up to 5% in LOI (Heiri et al. 2001). Gypsum, sulfide minerals, and metallic oxyhydroxides can modify LOI values as well, via oxidation or dehydration (Santisteban et al. 2004). But general trends of LOI show a good correlation with carbon content (both organic and inorganic) allowing use of LOI as a qualitative test for carbon content. Again, LOI shows a good correlation with other methods of determining

carbonate content of lake sediments (Dean 1974). Direct positive and significant correlation between LOI and total CaO ($r = 0.91$) in the Tagay sediments, means that LOI was mainly controlled by the carbonate content. Extreme contents of some elements observed in the samples retrieved from layers 4–6, 8–10, 15, and 17 (as numbered in Fig. 2) are associated both with variations in the mineral composition (e.g. limestones of layers 4 and 6) and with variations in the salinity and past acidic-alkaline and redox conditions.

Variations of major element weathering indices show the genetic homogeneity of the provenance rocks. High TM values suggest a nearby terrestrial matter source and the high ASM values make it possible to identify this source as weathering crust (Yudovich and Ketris 2000). Generally, the obtained values reflect the maturity of the studied sediments, which is confirmed by the low (less than 1) values of the ICV index (Cox et al. 1995).

Climatic conditions during formation of the Tagay sequence are not determined confidently by the bulk chemical composition of sediments. Thus, the median value of the HM is 0.42 with variations of 0.14–0.76. The chemical weathering intensity index CIA at a median value of 74 varies from 44 to 86. The lower values of indices are peculiar to carbonate deposits. Thus, the variation of this index reflects not only climatic changes during the formation of the sedimentary sequence, but also changes in the mineral composition. Generally, the HM and CIA values led us to conclude that the sequence sediments are products of a relatively temperate climate (Yudovich and Ketris 2000; Sheldon and Tabor

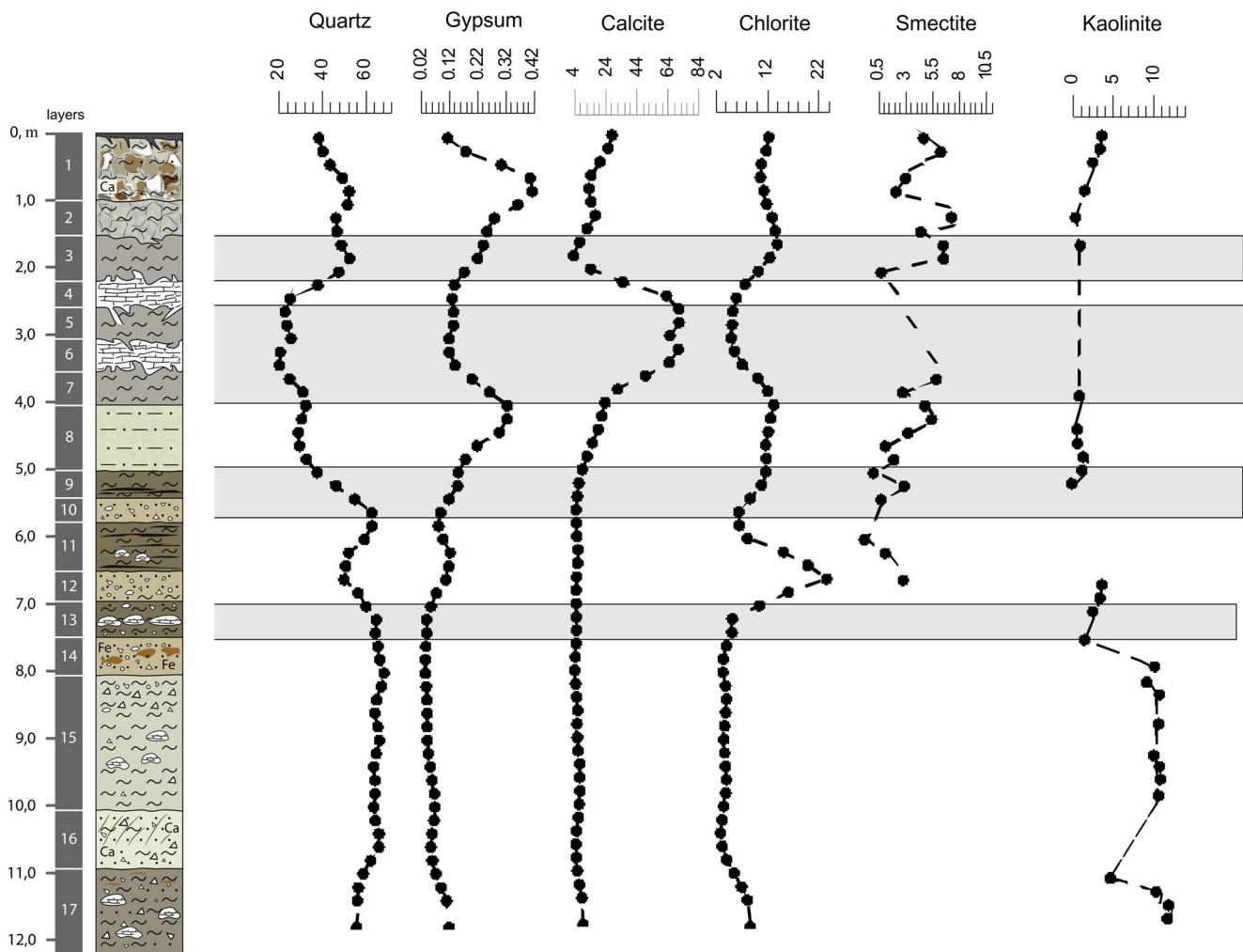


Fig. 7 Normative mineralogical calculations from bulk geochemistry of the Tagay sediments. Layers with fossil mammals are highlighted in grey.

2009). There is no significant correlation between the HM and CIA values, the correlation coefficient is 0.44.

CIA and weathering paths can also be evaluated using A–CN–K ($\text{Al}_2\text{O}_3\text{--CaO}^*\text{+Na}_2\text{O--K}_2\text{O}$) plots (Fig. 3). Most layers plot near the A-apex with relatively high CIA values (70–86), whereas those from less weathered sources plot with CIA values of 60–70. Ideal weathering trends (IWT) run from pristine source compositions near the feldspar join (CIA~50) parallel to the A–CN edge (Nesbitt and Young 1984). On the A–CN–K plot, most layers of the Tagay section do not diverge from their IWT, and trend toward smectite composition.

Figure 4(a) illustrates the K/Al and Mg/Al ratios. This graph shows a clear difference between the clayey rocks of the lower (layers 13, 15, and 17) and upper (layers 11–1) parts of the section. Clayey rocks in the lower part of the section have lower Mg/Al and K/Al ratios, which may be related to the presence of kaolinite. Rocks of the upper part of the section show elevated Mg/Al values, which may be associated with both the formation of magnesium carbonates and an increased role of terrigenous runoff (presence of chlorite). The

sediments of the upper part of the section are predominantly smectitic.

In the FM – NAM diagram (Fig. 4b), the composition points of the deposits form clusters. Most of the points fall in field II (mainly montmorillonite (smectite) with minor abundance of kaolinite and hydromica) and field I (mainly kaolinite clayey minerals). Several samples fall into field V (chlorite, montmorillonite, and hydromica (with abundant mixed-layer minerals)). This plot gives us the opportunity to have information about the original clay mineralogy.

In a binary $\text{K}_2\text{O}/\text{Al}_2\text{O}_3\text{--Ga/Rb}$ plot (Fig. 5) most samples fall in the field typical for the fine-grained clastic deposits of a warm and humid climate (Roy and Roser 2013). The same follows from the distribution of the samples in the Erofeev–Tsekhovskii diagram (Erofeev and Tsekhovskii 1983) (Fig. 6). Variations in the normative contents of quartz, calcite, gypsum, smectite, chlorite, and kaolinite through the Tagay profile (Fig. 7) also illustrate differences in the mineral composition of deposits in the upper and lower parts of the section.

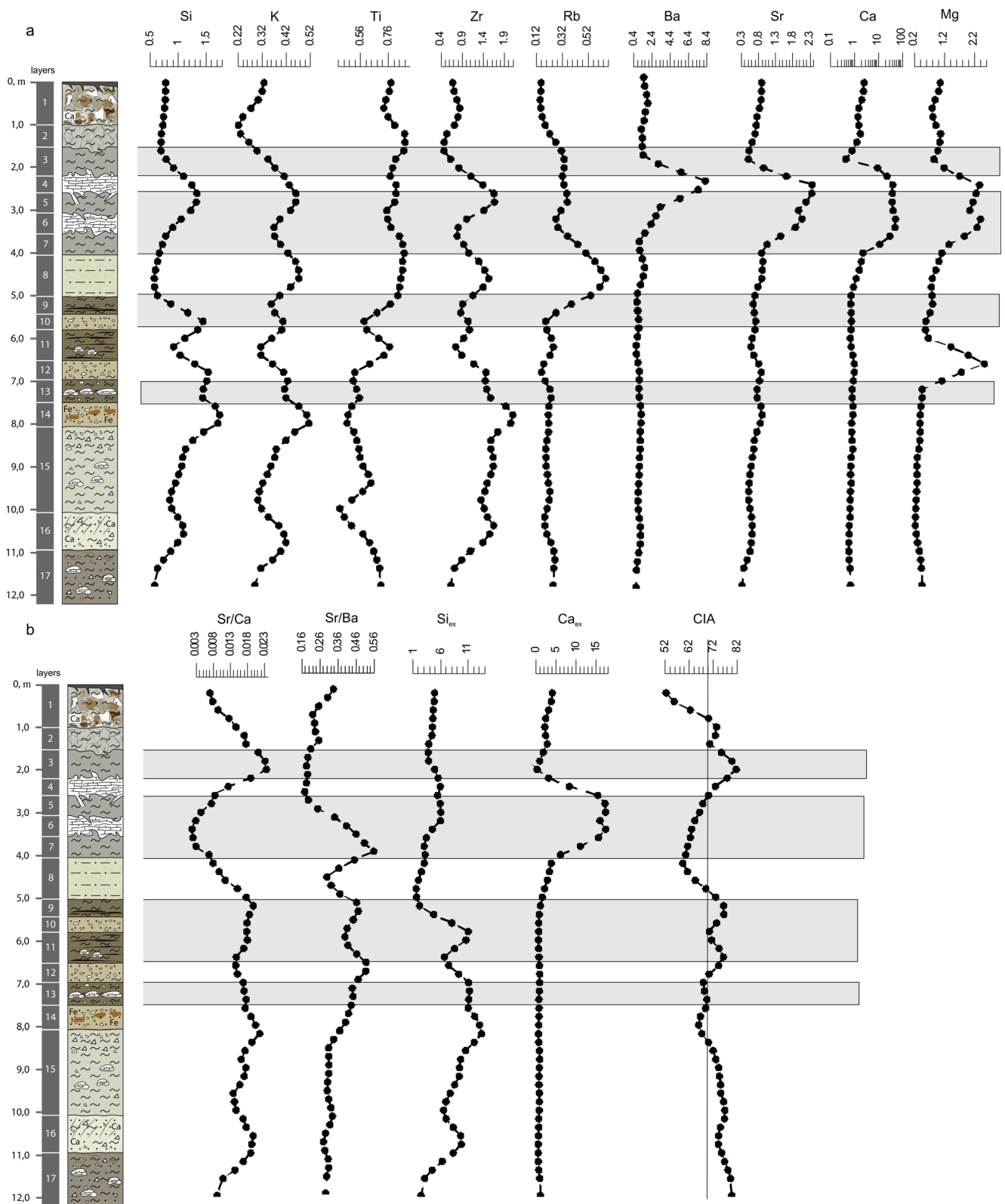


Fig. 8 **a** Distribution of the element enrichment factors through the Tagay profile. **b** Distribution of some element ratios, Si_{ex}, Ca_{ex} and CIA through the profile. All distribution curves were smoothed by the moving average method with a window of 4. Layers with fossil mammals are highlighted in grey

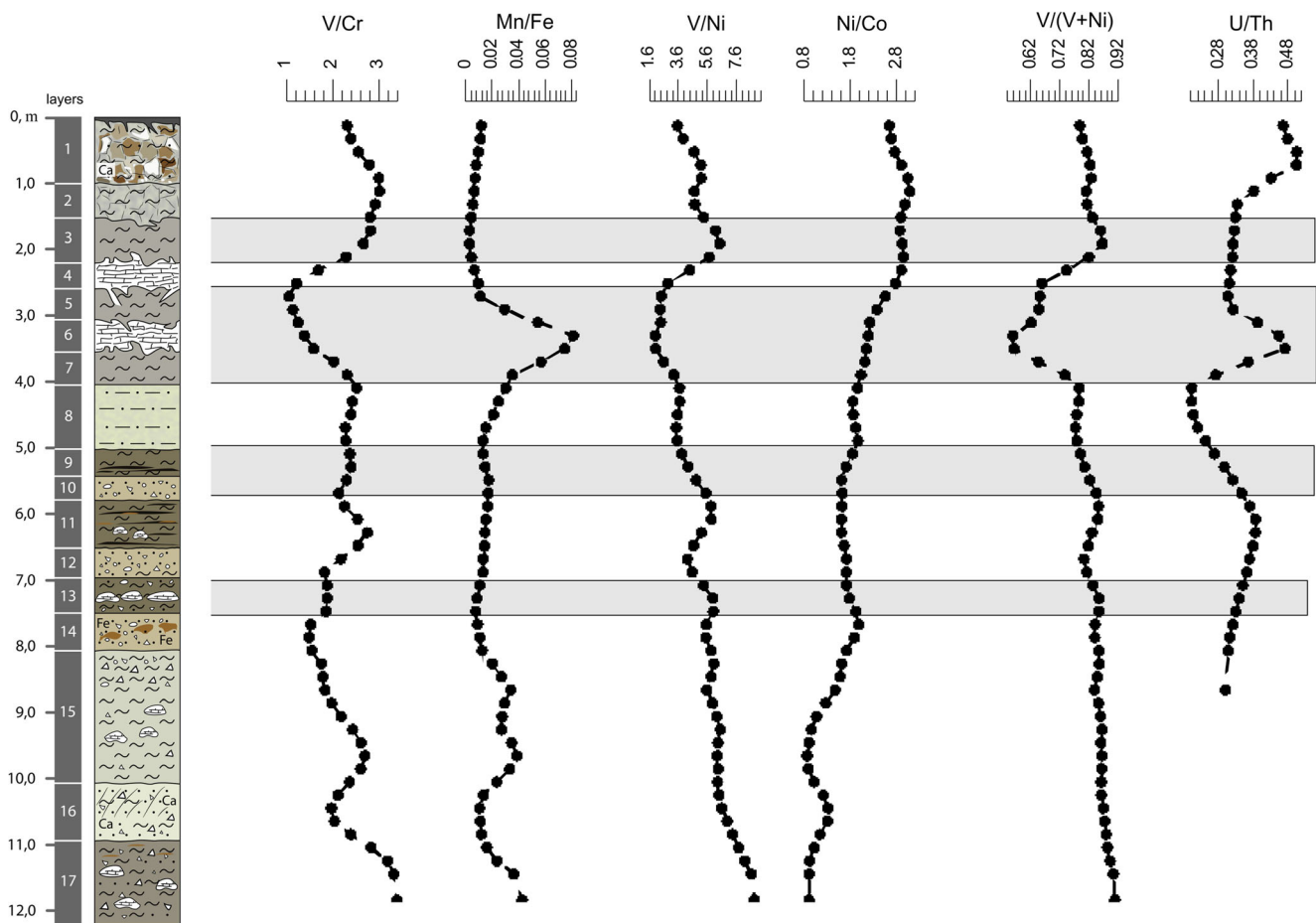


Fig. 9 Element ratio indicator for water redox conditions. Layers with fossil mammals are highlighted in grey

Fig. 10 Cross-correlation of V/Cr–Ni/Co. Layers are numbered according to the lithostratigraphic section in Fig. 2 (left)

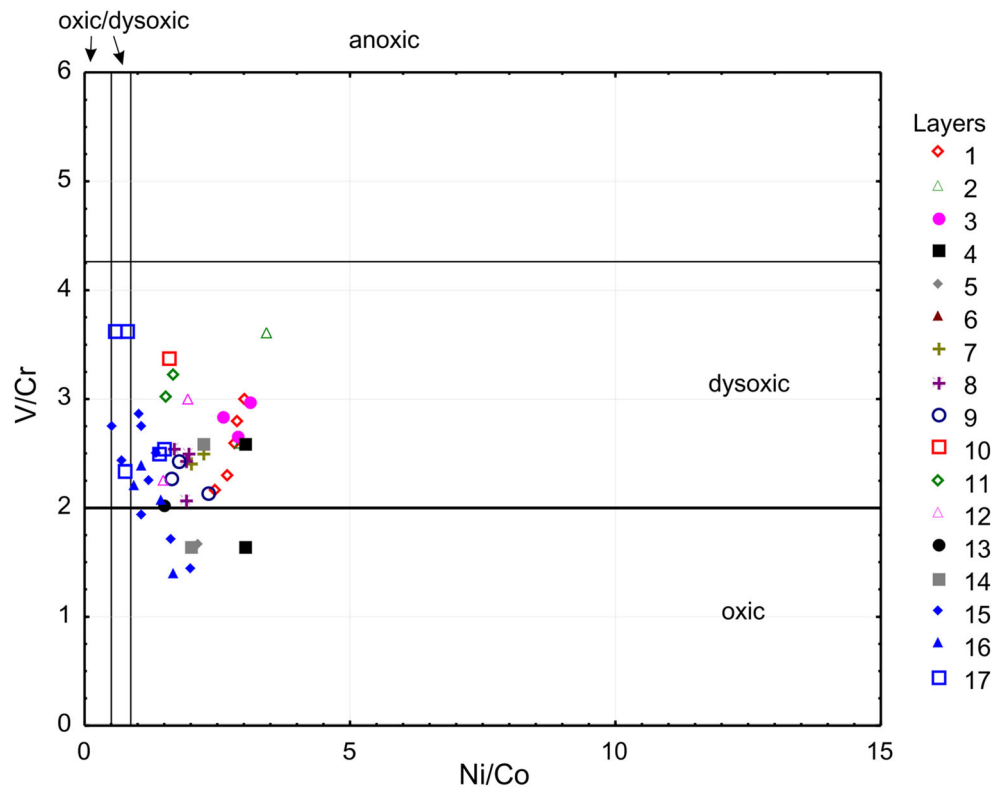


Table 5 REE content (ppm) and REE ratios in the Tagay-1 section sediments (18 samples)

Element/ratio	Mean	Minimum	Maximum	Std.Dev.	Coef.Var.
La	34.29	12.09	61.55	12.51	36
Ce	62.34	20.83	115.83	22.83	37
Pr	6.51	2.22	13.13	2.68	41
Nd	22.77	7.66	45.39	9.44	41
Sm	3.97	1.48	8.20	1.79	45
Eu	0.85	0.21	1.77	0.45	53
Gd	3.25	1.18	6.79	1.63	50
Tb	0.42	0.16	0.89	0.22	52
Dy	2.31	0.80	5.49	1.34	58
Ho	0.45	0.13	1.23	0.30	65
Er	1.28	0.35	3.70	0.89	69
Tm	0.19	0.05	0.55	0.13	70
Yb	1.25	0.36	3.61	0.87	70
Lu	0.18	0.06	0.52	0.12	67
Ce*	0.91	0.81	1.12	0.09	10
Eu*	1.01	0.70	1.23	0.16	16
LREE/HREE	2.84	1.25	6.87	1.42	50
LREE	126	43	236	47	37
MREE	11	4	24	6	50
HREE	3	1	8	2	69
Σ REE	140	49	266	53	38
Σ REE,Y	153	56	293	61	40
Σ Ce/ Σ Y	8.5	3.7	16.9	3.6	43
(La/Yb) _{NASC}	3.47	1.39	9.17	1.95	56
(La/Sm) _{NASC}	1.61	0.98	2.18	0.29	18
Pr*	1.06	0.90	1.14	0.06	6
t ₃	0.90	0.83	0.96	0.03	4
t ₄	1.03	0.95	1.10	0.04	4

The position of the samples in the binary K_2O/Al_2O_3 -Ga/Rb plot (Fig. 5) and the Erofeev-Tsekhovskii ternary plot (Fig. 6) in the field of humid climate deposits most likely illustrates the presence of unaltered source rocks in the dataset (Erofeev and Tsekhovskii 1983; Roy and Roser 2013). However, the sediments composition was undoubtedly influenced by changes in the acid-alkaline and redox conditions associated with periodic lowering of the lake's water level.

Variations of the enrichment factors for terrigenous (Si, K, Ti, Zr, Rb) and biogenic (Sr, Ca, Mg, Ba) elements in the Tagay profile (Table 4, Fig. 8 a) show that a relative increase in the terrigenous runoff in layers 5 and 8, 12, 15, and 16. The enrichment of sediments with biogenic elements increases in the layers 4-7 and 12 (Mg). During the accumulation of sediments in the lower part of the Tagay section (layers 17-9), the palaeo-lake level and salinity (Fig. 8 b) remained practically unchanged. Drawdown of the palaeo-lake and salinity increase began during the

formation of layer 8. The variations in the Sr/Ca and Mg/Ca coefficients testify to the minimum water level and maximum salinity during the deposition of layers 6 and 7. After the accumulation of layer 5, the water level began to rise, followed by a falling water level trend during the deposition of layer 3.

There is no correlation between the distributions of authigenic silica and calcium (Si_{ex} and Ca_{ex}). Increased Si_{ex} concentrations are observed in the lower part of the section (layers 17-10), other layers show a decreased Si_{ex} content. Increased contents of authigenic calcium were observed only in layers 5-7, where active carbonate deposition took place. Increased Si_{ex} contents may be associated with the presence of biogenic opal or chalcedony in the sediments and with the bio-productivity of the lake (diatoms).

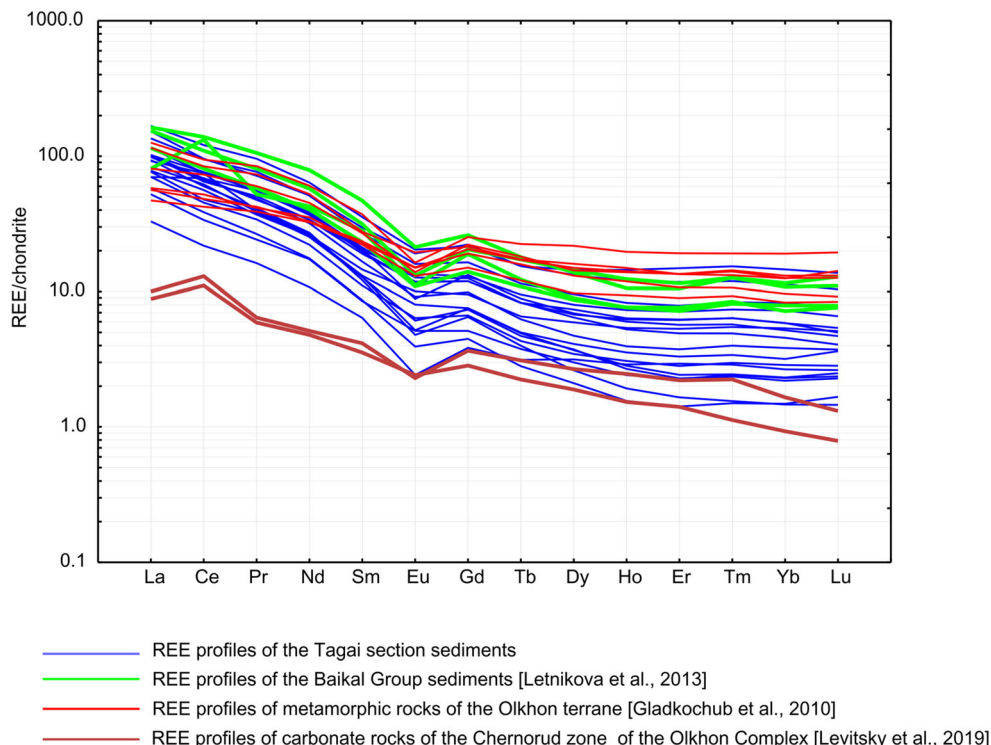
The trend of the CIA through the profile (Fig. 8b) shows that the sedimentary conditions were close to semiarid. The increased values of CIA mark humid periods, but high values above 80 more likely characterise the formation of the source area rocks (Sheldon and Tabor 2009). The assessment of the redox conditions of the sedimentary environment (Fig. 9) shows that they were fairly stable during the deposition of the Tagay sequence. The redox conditions varied from oxic to suboxic; dysoxic conditions were observed during the formation of layers 5-7 (Fig. 10). Thus, the formation of the sediment sequence of the Tagay section took place in fairly stable conditions of temperate climate, with alternating wet and semiarid phases.

Rare Earth Elements

REE values in Tagay-1 sediments suggest relatively stable geochemical properties during sediment deposition, and the overall similarity among REE patterns indicate a rather uniform provenance of the sediments (Taylor and McLennan 1985). Regarding their total REE content (49-266 ppm with average 140 ppm), the sediments do not differ from rocks of different genesis distributed on Olkhon Island: the REE content of the sandstones and siltstones of the Baikal Group ranges from 176 to 298 ppm, of the marbles of Olkhon Island from 22 to 25 ppm, and of the gneisses and granulites from 111 to 231 ppm (Gladkochub et al. 2010; Letnikova et al. 2013; Levitskiy et al. 2019). The lowest REE concentrations in the Tagay-1 sediments are seen in layers with high carbonate content.

Chondrite normalized REE patterns of the Tagay section and REE patterns of the Olkhon bedrocks (Fig. 11) show similar distribution curves with the enrichment of LREE and depletion of HREE. However, LREE excess is higher in the Tagay section than in the bedrocks: the LREE/HREE varies from 1.25 to 6.87; Σ Ce/ Σ Y varies from 3.6 to 16.9, while in bedrocks this ratio varies from 1.1 to 10.9. The removal of HREE occurs during the formation of weathering crust and

Fig. 11 Chondrite-normalised (Anders and Grevesse 1989) REE patterns in the Tagay section sediments compared with the REE patterns of various bedrocks of Olkhon Island



continues during the change of redox and acidic-alkaline conditions during diagenesis (Balashov 1976; Ivanova et al. 2020). The low values of the europium anomaly indicate the absence (or complete decomposition) of plagioclase in the sediments of the section.

The REE patterns of the Tagay sediments are potentially subject to secondary alteration during diagenetic exchange with either bottom or pore waters. The fractionated REE patterns and lack of correlation REE with Al, Fe, Ti, Mg and Zr content ($r < 0.5$) suggest that there is an additional REE source other than the terrigenous input.

REEs easily substitute for alkali metals and alkaline earths, adsorbed onto the surface and in the interlayer sites of clay minerals (Coppin et al. 2002). Moreover, both Mn and Fe oxyhydroxides are important REE scavengers in aquatic systems. REE adsorption/desorption is controlled by the nature of the minerals, as well as by pH and ionic strength of the solution. Saline waters (with high TDS (total dissolved solids)) have high ionic strength.

The fractionation of Ce from other REEs generally occurs in response to an oxidation reaction similar to the oxidation of Mn(II) to Mn(IV) (Bau, 1999). Because Ce^{4+} is less soluble

Fig. 12 Cerium versus praseodymium anomalies in the Tagay section sediments (NASC-normalised values, Gromet et al. 1984). True positive and negative cerium anomalies are provenance and redox proxies. Layers are numbered according to the lithostratigraphic section in Fig. 2 (left)

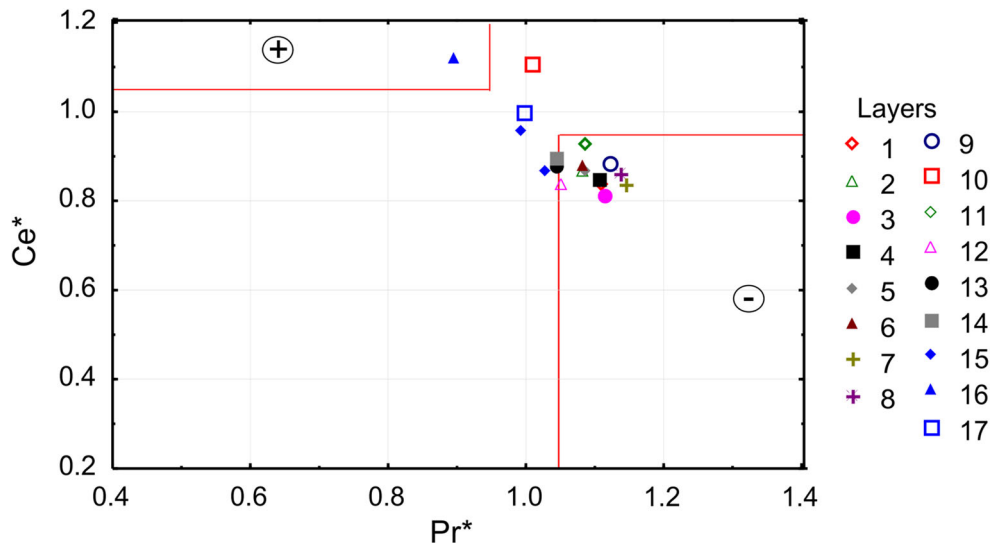
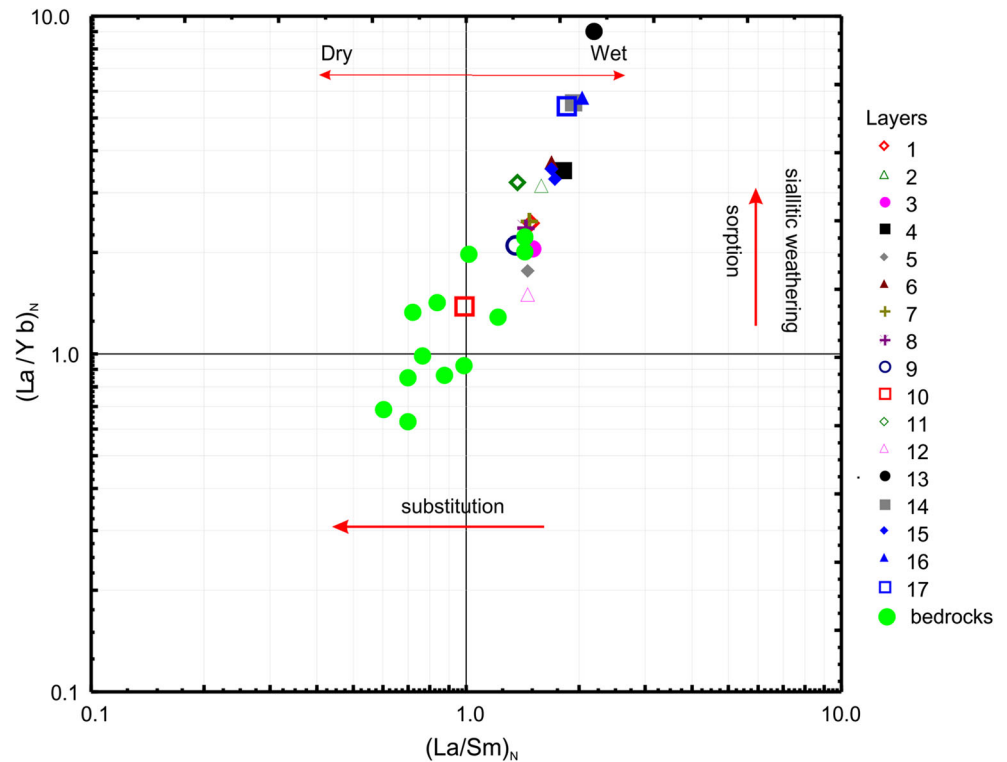


Fig. 13 Comparison of $(La/Sm)_N$ vs. $(La/Yb)_N$ ratios (NASC-normalized values, Gromet et al., 1984) in the Tagay sediments and Olkhon bedrocks (Gladkochub et al. 2010; Letnikova et al. 2013; Levitskiy et al., 2019). Layers are numbered according to the lithostratigraphic section in Fig. 2 (left)



than Ce^{3+} , Ce^{4+} can be removed from solution and then be incorporated into authigenic mineral phases.

Most true Ce anomalies in the Tagay sediments have small negative values (0.81-1.00, avg. 0.88) (Fig. 12). This can be explained by the mixing of various compo-

nents (essentially biogenic and authigenic) and of detrital materials (dominantly aluminosilicates) with crust-like Ce signatures. Och et al. (2014) suggested that the negative Ce anomaly observed in the sediments of Lake Baikal likely results from riverine transport due to either the successive

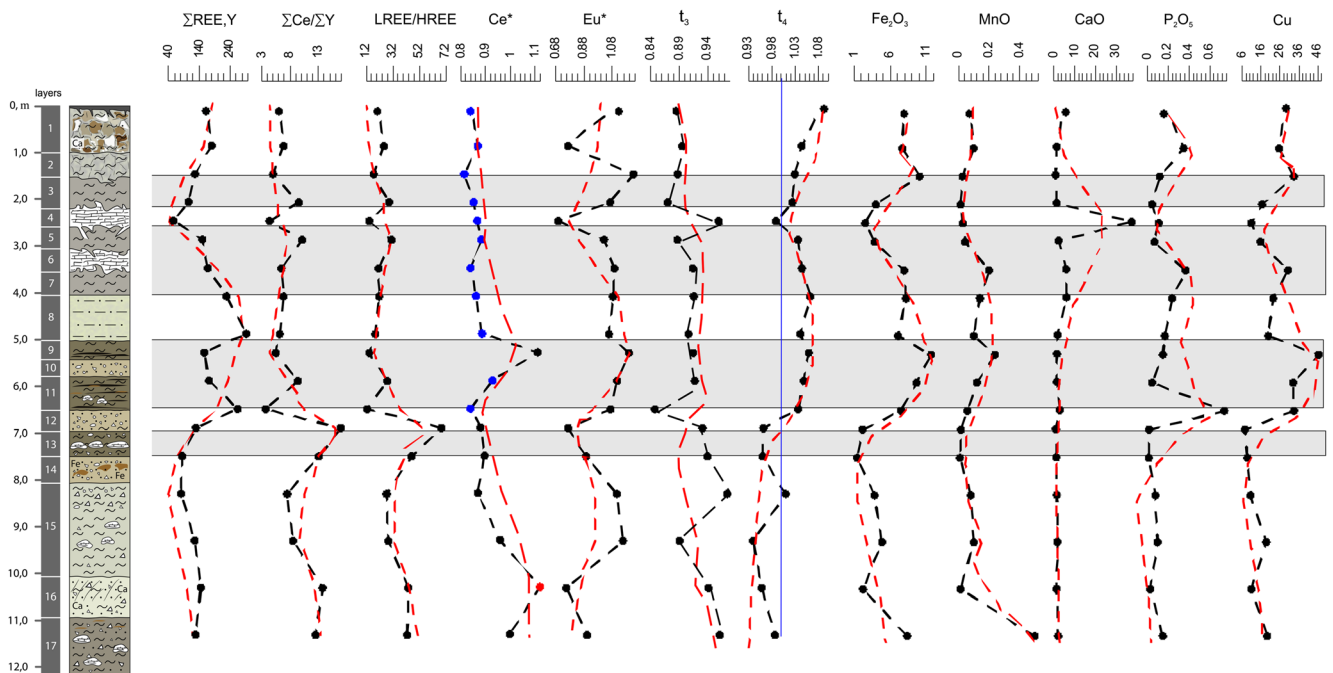


Fig. 14 Distribution of the REE geochemical indices, oxides and Cu through the Tagay profile. Red dashed lines mark change trends reconstructed by the moving average method with a window of 4; blue

points on the Ce^* profile correspond to true negative anomalies; the red point corresponds to a true positive anomaly. Layers with fossil mammals are highlighted in grey

retention of Ce within the river beds at a higher rate than the other REEs, or the higher solubility of Ce due to complex combination with organic ligands.

The true positive Ce anomaly in the sediments of the layer 16 (Fig. 12) is here suggested to have resulted from decreasing freshwater flow towards the palaeo-lake, thus leading to oxidative removal of Ce from the pore waters to the sediments (Hannigan et al. 2010). This suggested decrease might result from increasing aridity due to progressive decrease in effective precipitation in this area during the formation of the layer 16. These suggestions are consistent with the faunal record, which exhibits a lack of fossils in this unit. The remaining samples do not have true cerium anomalies, and therefore cannot be used in this type of depositional reconstruction.

Generally, REE accumulation in sediments is influenced by the isomorphic replacement of rock-forming mineral cations by REE cations, as well as by the sorption of REE by Fe (Mn)-rich oxyhydroxide colloids and clay minerals. LREE and MREE fractionation depends on the differences in their compound-forming ability in a water environment (Peppard et al. 1969). Increasing contents may be related to the partial scavenging of solutions during their percolation in the sedimentary sequence. The acquired $(La/Yb)_N - (La/Sm)_N$ ratio (Fig. 13) represents the continental (fluvial) setting of sedimentation (Trueman and Benton 1997; Trueman et al. 2006). The $(La/Yb)_N$ ratio varies within 1.39–9.17; the $(La/Sm)_N$ ratio varies within 0.98–2.18. Substitution is more important for the bedrocks. Apparently, sorption processes were leading in REE fractionation in the sediments (Trueman et al. 2006; Ivanova et al. 2020).

This supposition is also verified by the established tetrad-effect of lanthanoids for the third and fourth tetrad (Table 5, Fig. 14). The tetrad-effect of lanthanoids for the third tetrad is of the W-type for all sediments, but for the fourth tetrad varies from W-type (layers 17–13) to M-type (layers 12–1). Usually a W-type tetrad effect indicates REE dissolution, while the M-type indicate the REE association with a solid phase (or bacterial activity) (Masuda et al. 1987).

The correlation between distributions of iron and manganese oxides and tetrad-effect values is clearly visible in Fig. 14. It confirms the role of sorption in the process of REE fractionation (Masuda et al. 1987). Accordingly, the fractionation of medium and heavy lanthanides, associated with an increase in their migration ability with increasing alkalinity of the environment, is demonstrated for the Tagay sediments. The increased content of REE and yttrium in the layers 12–5 suggests a relatively high sedimentation rate (Balashov 1976). The geochemical profiles shown in Fig. 14 suggest that the middle part of the section (layers 12–5) was formed under the same conditions: in a weakly reducing and alkaline environment, which suggests some swamp conditions in the area.

Conclusions

The results of investigation of element content and major element weathering indices, their variations and their change over time, has led to the following conclusions:

- The removal of terrigenous material was mainly by surface runoff; hence, the sedimentary basin was mainly fed by erosion products of the weathering crust of the kaolinite and montmorillonite type. This factor determines the composition of the deposits.
- A relative increase in terrigenous runoff is observed in layers 5, 8, 12, 15, and 16.
- The enrichment of the sediments in biogenic elements is highest in layers 5–7 and 12.
- During sediment accumulation in the lower part of the Tagay section (layers 17–9), the palaeo-lake level and salinity remained practically unchanged.
- Drawdown of the palaeo-lake and a corresponding increase in salinity began during the deposition of layer 8.
- The minimum water level and maximum salinity were observed during the deposition of layers 6 and 7.
- Layers 6–8 were deposited in an arid environment.
- After the deposition of layer 5, the water level began to rise, but reversed to a falling trend during the formation of layer 3.
- The increased Si_{ex} contents may be associated with the presence of biogenic opal or chalcedony in the sediments and with the bioproductivity of the lake (diatoms).
- The assessment of the redox conditions of the sedimentary environment shows that they were fairly stable during the deposition of the Tagay sequence, and varied from oxic to suboxic.
- The increased content of REE and yttrium in layers 12–5 suggests a relatively high sedimentation rate during this interval.
- Most Ce anomalies in the Tagay sediments can be explained by mixing of various components (essentially biogenic and authigenic) and of detrital materials.
- The fractionation of medium and heavy lanthanides, associated with an increase in their migration ability with increasing alkalinity of the environment, is demonstrated for the Tagay sediments.
- The deposition of the sedimentary sequence of the Tagay section took place in fairly stable climatic and temperature conditions with alternating wet and semiarid phases.

It can be assumed that a) the deposition of the sediment sequence was relatively short in geological time; b) no abrupt climatic changes occurred.

Acknowledgements The research presented here was supported via research grants from the Russian Foundation for Basic Research (No. 20-05-00247), the Russian Science Foundation (No. 19-17-00216, sedimentology and geochemistry), and the Government of the Russian Federation (No. 075-15-2021-631), and was carried out in accordance with a State Assignment of the Vinogradov Institute of Geochemistry SB RAS (No. 0284-2021-0003). We warmly thank two anonymous reviewers for improving the manuscript.

Funding Open access funding provided by Swedish Museum of Natural History.

Data Availability All data generated or analysed during this study are included in this published article.

Declarations

Conflict of Interest The authors declare that they have no conflict of interest.

Open Access This article is licensed under a Creative Commons Attribution 4.0 International License, which permits use, sharing, adaptation, distribution and reproduction in any medium or format, as long as you give appropriate credit to the original author(s) and the source, provide a link to the Creative Commons licence, and indicate if changes were made. The images or other third party material in this article are included in the article's Creative Commons licence, unless indicated otherwise in a credit line to the material. If material is not included in the article's Creative Commons licence and your intended use is not permitted by statutory regulation or exceeds the permitted use, you will need to obtain permission directly from the copyright holder. To view a copy of this licence, visit <http://creativecommons.org/licenses/by/4.0/>.

References

- Anders, E., & Grevesse, N. (1989). Abundances of the elements: meteoric and solar. *Geochimica et Cosmochimica Acta*, 53, 197–214. [https://doi.org/10.1016/0016-7037\(89\)90286-X](https://doi.org/10.1016/0016-7037(89)90286-X)
- Balashov, Yu.A. (1976). *Geochemistry of the rare earth elements*. Moscow: Nauka. [in Russian]
- Bau, M. (1999). Scavenging of dissolved yttrium and rare earths by precipitating iron oxyhydroxide: experimental evidence for Ce oxidation, Y-Ho fractionation, and lanthanide tetrad effect. *Geochimica et Cosmochimica Acta* 63(1), 67–77.
- Bulkan, Ö., Toksoy, E.B., & Çağatay M. (2019). Geo-archives of a Coastal Lacustrine Eco-system: Lake Bafa (Mediterranean Sea). In G. Aiello (Ed.) *Sedimentary Processes Examples from Asia, Turkey and Nigeria* (pp.29–49). London: Intech Open.
- Čerňanský, A., Syromyatnikova, E.V., Kovalenko, E.S., Podurets, K.M., & Kaloyan, A.A. (2020). The key to understanding the European Miocene *Chalcides* (Squamata, Scincidae) comes from Asia: the lizards of the East Siberian Tagay locality (Baikal Lake) in Russia. *The Anatomical Record*, 303, 1901–1934.
- Coppin, F., Berger, G., Bauer, A., Castet, S., & Loubet, M. (2002). Sorption of lanthanides on smectite and kaolinite. *Chemical Geology*, 182, 57–68.
- Cox, R., Lowe, D.R., & Cullers, R.L. (1995). The influence of sediment recycling and basement composition on evolution of mudrock chemistry in southwestern United States. *Geochimica et Cosmochimica Acta*, 59, 2919–2940. [https://doi.org/10.1016/0016-7037\(95\)00185-9](https://doi.org/10.1016/0016-7037(95)00185-9).
- Danilov, I.G., Syromyatnikova, E.V., & Hirayama, R. (2012). Fossil turtles of the genus *Baicalemys* (Emyidae): new data on morphology and phylogenetic position (preliminary results). In N.B. Ananieva, E.A. Kulikova, R.V. Novitskij, & V.V. Ustin (Eds.), *The problems of herpetology. Proceedings of the 5th Congress of the Alexander M. Nikolsky Herpetological Society* (pp. 68–71). Minsk: Pravo i Ekonomika Publ. [in Russian]
- Daxner-Höck, G., Böhme, M., & Kossler, A. (2013). New Data on the Miocene Biostratigraphy and Paleoclimatology of Olkhon Island (Lake Baikal, Siberia). In X.-M. Wang, L. J Flynn, & M. Fortelius (Eds.), *Fossil Mammals of Asia. Neogene biostratigraphy and chronology* (pp. 508–517). New York: University Press. <https://doi.org/10.7312/columbia/9780231150125.003.0022>.
- Daxner-Höck, G., Mörs, T., Kazansky, A.Y., Matasova, G.G., Ivanova, V.V., Shchetnikov, A.A., Filinov, I.A., Voyta, L., & Erbajeva, M.A. (2022). A synthesis of fauna, palaeoenvironments and stratigraphy of the Miocene Tagay locality (Olkhon Island, Lake Baikal, Eastern Siberia). In G. Daxner-Höck, & A. A. Shchetnikov (Eds.), *The Miocene Tagay locality of Olkhon Island (Lake Baikal, Eastern Siberia) – a multidisciplinary approach. Palaeobiodiversity and Palaeoenvironments* 102(4). <https://doi.org/10.1007/s12549-022-00558-8>. [this issue]
- Dean, W.E. (1974). Determination of carbonate and organic matter in calcareous sediments and sedimentary rocks by loss on ignition: comparison with other methods. *Journal of Sedimentary Petrology*, 44: 242–248.
- Dia, A., Gruau, G., Olivie-Lauquet, G., Riou, C., Molénat, J., & Curmi, P. (2000). The distribution of rare earth elements in groundwaters: assessing the role of source rock composition, redox changes, and colloidal particles. *Geochimica et Cosmochimica Acta*, 64, 4131–4152. [https://doi.org/10.1016/S0016-7037\(00\)00494-4](https://doi.org/10.1016/S0016-7037(00)00494-4).
- Erbajeva M, & Alexeeva N. (2013). Late Cenozoic Mammal Faunas of the Baikalian Region: Composition, Biochronology, Dispersal, and Correlation with Central Asia. In X.-M. Wang, L. J., Flynn, & M. Fortelius, (Eds.), *Fossil Mammals of Asia. Neogene biostratigraphy and chronology* (pp. 495–507). New York: University Press. <https://doi.org/10.7312/columbia/9780231150125.003.0022>.
- Erofeev, V.S., & Tsekhovskii, Yu.G. (1983). *Parageneses of Continental Deposits*. Moscow: Nauka. [in Russian]
- Filippov, A. G., Erbajeva, M. A., & Sychevskaya, E. K. (2000). Remains of snake-headed Fishes (Channidae) near Baikal. *Third Vereshchagin's Baikal conference. Irkutsk: Limnological Institute*, 251.
- Gladkochub, D.P., Donskaya, T.V., Fedorovsky, V.S., Mazukabzov, A.M., Larionov, A.N., & Sergeev, S.A. (2010). The Olkhon metamorphic terrane in the Baikal region: An Early Paleozoic collage of Neoproterozoic active margin fragments. *Russian Geology and Geophysics*, 51(5), 447–460. <https://doi.org/10.1016/j.rgg.2010.04.001>.
- Gromet, L.P., Dymek, R.F., Haskin, L.A., & Korotev, R.L. (1984). The North American Shale Composite: Its composition, major, and trace element characteristics. *Geochimica et Cosmochimica Acta*, 48, 2469–2482. [https://doi.org/10.1016/0016-7037\(84\)90298-9](https://doi.org/10.1016/0016-7037(84)90298-9).
- Hannigan, R., Dorval, E., & Jones, C. (2010). The rare earth element chemistry of estuarine surface sediments in the Chesapeake Bay. *Chemical Geology*, 272(1–4), 20–30. <https://doi.org/10.1016/j.chemgeo.2010.01.009>.

- Heiri, O., Lotter, A.F. & Lemcke, G. (2001). Loss on ignition as a method for estimating organic and carbonate content in sediments: reproducibility and comparability of results. *Journal of Paleolimnology*, 25, 101–110.
- Heymann, C., Nelle, O., Dorfler, W., Zagana, H., Nowaczyk, N., Xue, J., & Unkel, I. (2013). Late Glacial to mid-Holocene palaeoclimate development of southern Greece inferred from the sediment sequence of Lake Stymphalia (NE-Peloponnese). *Quaternary International*, 302, 42–60. <https://doi.org/10.1016/j.quaint.2013.02.014>.
- Irber, W. (1999). The lanthanide tetrad effect and its correlation with K/Rb, Eu/Eu*, Sr/Eu, Y/Ho, and Zr/Hf of evolving peraluminous granite suites. *Geochimica et Cosmochimica Acta*, 63, 489–508. [https://doi.org/10.1016/S0016-7037\(99\)00027-7](https://doi.org/10.1016/S0016-7037(99)00027-7).
- Ivanova, V.V., Erbajeva, M.A., Shchetnikov A.A., Kazansky A.Y., Matasova G.G., Alekseeva, N.V., Filinov I.A., & Kuzmin, M.I. (2020). The Tologoi Key Section (Upper Cenozoic, Transbaikalia): Reconstruction of the Peculiarities and Depositional Environment. *Russian Geology and Geophysics*, 61(12), 1374–1390. <https://doi.org/10.15372/RGG2020141>.
- Kackstaetter, U.R. (2014). SEDMIN - Microsoft Excel™ spreadsheet for calculating fine-grained sedimentary rock mineralogy from bulk geochemical analysis. *Central European Journal of Geosciences*, 6 (2), 170–181. <https://doi.org/10.2478/s13533-012-0170-3>.
- Kitaynik, A.F. (1958). *Note on Tertiary Deposits of Olkhon Island on Lake Baikal* (pp. 55–60). Irkutsk: Zapiski IOKM. [in Russian]
- Klementiev A.M. & Sizov A.V. (2015). New record of anchithere (*Anchitherium aurelianense*) in the Miocene of eastern Siberia, Russia. *Russian Journal of Theriology*, 14(2), 133–143.
- Kossler, A. (2003). Neogene Sediments of Olkhon and Svyatoy Nos (Baikal Rift System, East Siberia): Suggestions about the Development of Lake Baikal. *Berliner Paläobiologische Abhandlungen*, 4, 55–63.
- Kučera, J., Cempírek, J., Dolníček, Z., Muchez, P., & Prochaska, W. (2009). Rare earth elements and yttrium geochemistry of dolomite from post-Variscan vein-type mineralization of the Nizký Jeseník and Upper Silesian Basins, Czech Republic. *Journal of Geochemical Exploration*, 103(2–3), 69–79. <https://doi.org/10.1016/j.gexplo.2009.08.001>.
- Letnikova, E.F., Kuznetsov, A.B., Vishnevskaya, I.A., Veshcheva, S.V., Proshenkin, A.I., & Geng, H. (2013). The Vendian passive continental margin in the southern Siberian Craton: Geochemical and isotopic (Sr, Sm-Nd) evidence and U-Pb dating of detrital zircons by the LA-ICP-MS method. *Russian Geology and Geophysics*, 54(10), 1177–1194. <https://doi.org/10.1016/j.rgg.2013.09.004>.
- Levitskiy, V.I., Levitskiy, I.V., Reznitskiy, & L.Z. (2019). Geochemistry of carbonate rocks in the Early Precambrian and Phanerozoic metamorphic complexes of East Siberia, north-west Russia, and Pamirs. *Geochemistry International*, 57(4), 438–455. <https://doi.org/10.1134/S0016702919040074>.
- Logachev, N.A., Lomonosova, T.K., & Klimanova, V.M. (1964). *Cenozoic deposits of the Irkutsk Amphitheatre* (pp. 1–196). Moscow: Nauka. [in Russian]
- Logachev, N.A. (1974). Sayano-Baikal Stanovoe Upland. *Uplands of the Baikal and Transbaikali* (pp. 1–360). Moscow: Nauka. [in Russian]
- Maslov, A.V. (2005). *Sedimentary Rocks: Methods for the Study and Interpretation of Obtained Data*, Yekaterinburg: UGGU, 2005. [in Russian]
- Maslov, A.V., Krupenin, M.T., Petrov, G.A., Ronkin, Yu.L., Lepikhina, O.P., & Kornilova, A.Yu. (2007). Certain geochemical features and conditions of sedimentation of fine-grained terrigenous rocks of Serebryanka and Sylvitsa groups (Middle Urals). *Litosfera*, 2, 3–28.
- Masuda, A., Kawakami, O., Dohmoto, Y., & Takenaka, T. (1987). Lanthanide tetrad effects in nature: Two mutually opposite types, W and M. *Geochemical Journal*, 21, 119–124. <https://doi.org/10.2343/geochemj.21.119>.
- Mats, V.D., Pokatilov, A.G., & Popova, S.M. (1982). *Pliocene and Pleistocene of Middle Baikal* (pp. 1–193). Novosibirsk: Nauka. [in Russian]
- Mats, V.D., Ufimtsev G.F., Mandelbaum M.M., Alakshin A.M., Pospeev A.V., Shimaraev M.N., & Khlystov O.M. (2001). *The Cenozoic of the Baikal Rift Basin: Structure and geological history* (pp. 1–252). Novosibirsk: Geo. [in Russian]
- Mats, V.D., Lomonosova, T.K., Vorobjeva, G.A., & Vologina, E.G. (2010). Late Cretaceous-Cenozoic sediments of the Baikal rift basin and changing natural conditions. *Geodynamics and Tectonophysics*, 1(1), 75–86. <https://doi.org/10.5800/GT-2010-1-1-0007>. [in Russian]
- Mats, V.D., Shcherbakov, D.Y., & Efimova, I.M. (2011). Late Cretaceous–Cenozoic History of the Lake Baikal Depression and Formation of its Unique Biodiversity. *Stratigraphy and Geological Correlation*, 19/4, 404–423. Pleiades Publishing Ltd. ISSN 0869-5938.
- McLennan, S.M. (1994). Rare earth element geochemistry and the "tetrad" effect. *Geochimica et Cosmochimica Acta*, 58, 2025–2033. [https://doi.org/10.1016/0016-7037\(94\)90282-8](https://doi.org/10.1016/0016-7037(94)90282-8).
- McLennan, S.M., Hemming, S., McDaniel, D.K., & Hanson, G.N. (1993). Geochemical approaches to sedimentation, provenance, and tectonics. In M. J. Johnsson, A. Basu (Eds.), *Processes controlling the composition of clastic sediments. Geological Society of America Special Paper*, 284, 21–40. <https://doi.org/10.1130/SPE284-p21>.
- Nesbitt, H.W. (2003). Petrogenesis of siliciclastic sediments and sedimentary rocks. In D. R. Lentz (Ed.), *Geochemistry of sediments and sedimentary rocks: evolutionary considerations to mineral deposit-forming environments. Geological Association of Canada, GeoText*, 4, 39–51.
- Nesbitt, H.W., & Young, G.M. (1982). Early Proterozoic climates and plate motions inferred from major element chemistry of lutites, *Nature*, 299, 715–717. <https://doi.org/10.1038/299715a0>.
- Nesbitt, H.W., & Young, G.M. (1984). Prediction of some weathering trends of plutonic and volcanic rocks based on thermodynamic and kinetic considerations, *Geochimica et Cosmochimica Acta*, 48(7), 1523–1534. [https://doi.org/10.1016/0016-7037\(84\)90408-3](https://doi.org/10.1016/0016-7037(84)90408-3).
- Och, L. M., Müller, B., Wichser, A., Ulrich, A., Vologina, E. G., & Sturm, M. (2014). Rare earth elements in the sediments of Lake Baikal. *Chemical Geology*, 376, 61–75. <https://doi.org/10.1016/j.chemgeo.2014.03.018>.
- Panteeva, S.V., Gladkochoub, D.P., Donskaya, T.V., Markova, V.V., & Sandimirova, G.P. (2003). Determination of 24 trace elements in felsic rocks by inductively coupled plasma mass spectrometry after lithium metaborate fusion. *Spectrochimica Acta Part B: Atomic Spectroscopy*, 58 (2), 341–350. [https://doi.org/10.1016/S0584-8547\(02\)00151-9](https://doi.org/10.1016/S0584-8547(02)00151-9).
- Pashkova, G.V., Aisueva, T.S., Finkelshtein, A.L., Cherkashina, T., & Shchetnikov, A.A. (2018). Quantitative approaches to the determination of elements in lake sediments by total reflection X-ray fluorescence. *Microchemical Journal*, 143, 264–271. <https://doi.org/10.1016/j.microc.2018.08.020>.
- Patrick, D., Martin, J. E., Parris, D. C., & Grandstaff, D. E. (2004). Paleoenvironmental interpretations of rare earth element signatures in mosasaurs (Reptilia) from the upper Cretaceous Pierre Shale, central South Dakota, USA. *Palaeogeography, Palaeoclimatology, Palaeoecology*, 212, 277–294. [https://doi.org/10.1016/S0031-0182\(04\)00315-3](https://doi.org/10.1016/S0031-0182(04)00315-3).
- Peinerud, E., Ingri, J., & Pontér, C. (2001). Non-detrital Si concentrations as an estimate of diatom concentrations in lake sediments and suspended material. *Chemical Geology*, 177(3–4), 229–239. [https://doi.org/10.1016/s0009-2541\(00\)00378-8](https://doi.org/10.1016/s0009-2541(00)00378-8).
- Peppard, D.F., Mason, G.W., & Lewey, S. (1969). A tetrad effect in the liquid-liquid extraction ordering of lanthanides (III). *Journal of*

- Inorganic and Nuclear Chemistry*, 31, 2271–2272. [https://doi.org/10.1016/0022-1902\(69\)90044-X](https://doi.org/10.1016/0022-1902(69)90044-X).
- Pettijohn, F.J. (1975). *Sedimentary Rocks*. New York: Harper and Row.
- Pokatilov, A.G. (2004). *Paleontology and stratigraphy of the Cenozoic in the south of Eastern Siberia and adjacent territories*. Irkutsk: Izd-vo ISTU. [in Russian]
- Retallack, G.J. (2001). *Soils of the Past: an Introduction to Paleopedology*. Oxford: Blackwell.
- Retallack, G.J. (2007). Soils and Global Change in the Carbon Cycle over Geological Time. *Treatise On Geochemistry*, 581–605.
- Roy, D.K., & Roser, B.P. (2013). Climatic control on the composition of Carboniferous-Permian Gondwana sediments, Khalaspir basin, Bangladesh. *Gondwana Resources Limited*, 23(3), 1163–1171. <https://doi.org/10.1016/j.gr.2012.07.006>.
- Santisteban, J.I., Mediavilla, R., Lopez-Pamo, E., Dabrio, C.J., Zapata, M.B.R., Garcia, M.J.G., Castano, S., & Martinez-Alfaro, P. E. (2004). Loss on ignition: a qualitative or quantitative method for organic matter and carbonate mineral content in sediments? *Journal of Paleolimnology*, 32, 287–299. <https://doi.org/10.1023/B:JOPL.0000042999.30131.5b>.
- Sheldon, N.D. (2006). Abrupt chemical weathering increase across the Permian-Triassic boundary. *Palaeogeography, Palaeoclimatology, Palaeoecology* 231, 315–321. <https://doi.org/10.1016/j.palaeo.2005.09.001>.
- Sheldon, N.D., & Tabor, N.J. (2009). Quantitative paleoenvironmental and paleoclimatic reconstruction using paleosols. *Earth-Science Reviews*, 95, 1–52. <https://doi.org/10.1016/j.earscirev.2009.03.004>.
- Sizov, A.V., & Klementiev, A.M. (2015). Geology and taphonomy of Tagay locality of early Miocene vertebrate fauna. In E. A. Lipnina, & I. M. Berdnikov (Eds.), *Eurasia in the Cenozoic. Stratigraphy, paleoecology, cultures. No. 4* (pp. 206–218). Irkutsk: Irkutsk State University Press. [in Russian]
- Sotnikova, M., Klementiev, A., Sizov, A., & Tesakov, A. (2019). New species of *Ballusia* Ginsburg and Morales, (Ursidae, Carnivora) from Miocene of Eastern Siberia, Russia. *Historical Biology*, <https://doi.org/10.1080/08912963.2019.1637864>.
- Syromyatnikova, E.V. (2014). The first record of *Salamandrella* (Caudata: Hynobiidae) from the Neogene of Russia. *Russian Journal of Herpetology*, 21(3), 217–220.
- Syromyatnikova, E.V. (2015). A new species of *Bufo* (Amphibia, Anura) from the Miocene of Russia. *Russian Journal of Herpetology* 22(4), 281–288.
- Syromyatnikova, E.V. (2016). Anurans of the Tagay locality (Baikal Lake, Russia; Miocene): Bombinatoridae, Hylidae, and Ranidae. *Russian Journal of Herpetology* 23(2), 145–157.
- Taylor, S.R., & McLennan, S.M. (1985). *The Continental Crust; Its composition and evolution; an examination of the geochemical record preserved in sedimentary rocks*. Oxford: Blackwell.
- Tesakov, A.S., & Lopatin, A.V. (2015). First record of mylagaulid rodents (Rodentia; Mammalia) from the Miocene of Eastern Siberia (Olkhon Island, Baikal Lake, Irkutsk Region, Russia). *Doklady Biological Sciences*, 460, 23–26.
- Trueman, C.N., & Benton, M.J. (1997). A geochemical method to trace the taphonomic history of reworked bones in sedimentary settings. *Geology*, 5, 263–266. [https://doi.org/10.1130/0091-7613\(1997\)025<0263:AGMTT>2.3.CO;2](https://doi.org/10.1130/0091-7613(1997)025<0263:AGMTT>2.3.CO;2).
- Trueman, C.N., Behrensmeyer, A.K., Potts, R., & Tuross, N. (2006). High-resolution records of location and stratigraphic provenance from the rare earth element composition of fossil bones. *Geochimica et Cosmochimica Acta*, 70, 4343–4355. <https://doi.org/10.1016/j.gca.2006.06.1556>.
- Turgeon, S., & Brumsack, H.J. (2006). Anoxic vs dysoxic events reflected in sediment geochemistry during the Cenomanian Turonian Boundary Event (Cretaceous) in the Umbria Marche Basin of central Italy. *Chemical Geology*, 234, 321–339. <https://doi.org/10.1016/j.chemgeo.2006.05.008>.
- Vislobokova, I.A. (1990). O parnopalykh iz nizhnego miotsena bukhty Tagay o. Ol'khon (Baykal). *Paleontological Journal*, 2, 134–138. [in Russian]
- Vislobokova, I.A. (1994). The Lower Miocene artiodactyls of Tagay Bay, Olkhon Island, Lake Baikal (Russia). *Palaeovertebrata*, 23, 177–197.
- Vislobokova, I.A. (2004). New species of *Orygotherium* (Palaeomerycidae, Ruminantia) from the Early and Late Miocene of Eurasia. *Annalen des Naturhistorischen Museums Wien, Serie A*, 106, 371–385.
- Volkova, N.V. (2020). The first barbets (Aves, Ramphastidae) from Siberia. *Journal of Ornithology*, 161, 325–332.
- Wedepohl, K.H. (1991). The composition of the upper Earth's crust and the natural cycles of selected elements. Metals in natural raw materials. Natural resources. In E. Merian (Ed.), *Metals and their Compounds in the Natural Environment* (pp. 3–17). Weinheim, Germany: VCH.
- Yudovich, Y.E., & Ketris, M.P. (2000). *Principles of Lithochemistry*. St. Petersburg: Nauka. 479 c. [in Russian]
- Zelenkov, N.V. (2015). A primitive grebe (Aves, Podicipedidae) from the Miocene of Eastern Siberia (Lake Baikal, Olkhon Island). *Paleontological Journal*, 49(5), 521–529.
- Zelenkov, N.V. (2016a). Evolution of bird communities in the Neogene of Central Asia, with a review of the Neogene fossil record of Asian birds. *Paleontological Journal*, 50(6), 1–6.
- Zelenkov, N.V. (2016b). The first fossil parrot (Aves, Psittaciformes) from Siberia and its implications for the historical biogeography of psittaciformes. *Biology Letters*, 12, 1–4.
- Zelenkov, N.V., & Martynovich, N.V. (2013). A rich bird fauna from the Miocene locality Tagay (Olkhon Island, Baikal Lake). *Arch Menzbier Ornithol Soc* 2, 73–93. [in Russian]
- Zelenkov, N.V., Stidham T.A. Martynovich, N.V., Volkova, N.V., Li, Q., & Qiu, Z. (2018). The middle Miocene duck *Chenoanas* (Aves, Anatidae): new species, phylogeny and geographical range. *Papers in Paleontology*, 4(3), 309–326.
- Zhao, Z.X., Dong, C.M., Lin, C.Y., Zhang, X.G., Huang, X., & Li, B.J. (2019). Sedimentary environment and facies of the Huangang formation in the northern central Xihu depression, east China sea basin, China. *Journal of the Geological Society of Australia* 67(3), 379–392.